1-1-1998

Thermal stress analysis of thermally sprayed coatings on a spent nuclear fuel waste package

Michael Joseph Plinski
University of Nevada, Las Vegas

INFORMATION TO USERS

This manuscript has been reproduced from the microfilm master. UMI films the text directly from the original or copy submitted. Thus, some thesis and dissertation copies are in typewriter face, while others may be from any type of computer printer.

The quality of this reproduction is dependent upon the quality of the copy submitted. Broken or indistinct print, colored or poor quality illustrations and photographs, print bleedthrough, substandard margins, and improper alignment can adversely affect reproduction.

In the unlikely event that the author did not send UMI a complete manuscript and there are missing pages, these will be noted. Also, if unauthorized copyright material had to be removed, a note will indicate the deletion.

Oversize materials (e.g., maps, drawings, charts) are reproduced by sectioning the original, beginning at the upper left-hand corner and continuing from left to right in equal sections with small overlaps. Each original is also photographed in one exposure and is included in reduced form at the back of the book.

Photographs included in the original manuscript have been reproduced xerographically in this copy. Higher quality 6" x 9" black and white photographic prints are available for any photographs or illustrations appearing in this copy for an additional charge. Contact UMI directly to order.

UMI

A Bell & Howell Information Company
300 North Zeeb Road, Ann Arbor MI 48106-1346 USA
313/761-4700 800/521-0600

THERMAL STRESS ANALYSIS OF THERMALLY SPRAYED COATINGS ON A SPENT NUCLEAR FUEL WASTE PACKAGE

by

Michael Joseph Plinski

Bachelor of Science
University of Nevada, Las Vegas
1995

A thesis submitted in partial fulfillment
of the requirements for the degree of

Master of Science

in

Mechanical Engineering

Department of Mechanical Engineering
University of Nevada, Las Vegas
May 1998

UNLV

Thesis Approval
The Graduate College
University of Nevada, Las Vegas

November 24, 19 97

The Thesis prepared by
Michael Joseph Plinski

Entitled

Thermal Stress Analysis of Thermally Sprayed Coatings on a Spent Nuclear Fuel Waste Package

is approved in partial fulfillment of the requirements for the degree of

Master of Science in Mechanical Engineering

Darrell W. Pepper
Examination Committee Chair

Penny Amy
Dean of the Graduate College

Robert Seeger
Examination Committee Member

B. J. Stook
Examination Committee Member

Michelle Schantz
Graduate College Faculty Representative

ABSTRACT

Thermal Stress Analysis of Thermally Sprayed

Coatings on a Spent Nuclear Fuel Waste Package

by

Michael Joseph Plinski

Dr. Darrell W. Pepper, Examination Committee Chair
Professor of Mechanical Engineering
University of Nevada, Las Vegas

The purpose of applying a thermal sprayed coating on a spent nuclear fuel waste package is to prevent moisture contacting the spent nuclear fuel for tens of thousands of years. This thesis studies some of the thermal effects that a coated waste package may experience. Residual stress from the thermal spray process is one of these effects and in this study two modeling methods are compared. Finally, a finite element analysis of the initial emplacement of the spent nuclear fuel in the waste package is used to determine if any spalling of the coating from the waste package will occur.

The results of the residual stress study and the thermal stress study indicate that all of the coatings will not spall off from the waste package. The ceramic coatings have the lowest stress values out of the three material cases. Therefore, future studies are needed to develop this design option for the waste package development.

TABLE OF CONTENTS

LIST OF FIGURES

LIST OF TABLES

ACKNOWLEDGMENTS

I would like to give my appreciation to the Management and Operating Contractor for the Mined Geologic Disposal System for allowing me to perform this study. I need to give a very special thanks to the Waste Package Development Group for the support they gave me on this undertaking. Finally, I appreciate all the efforts that all my professors, staff, and students of the University of Nevada, Las Vegas gave me on my educational pursuit.

CHAPTER 1

INTRODUCTION

The United States Department of Energy, Office of Civilian Radioactive Waste Management and Management and Operating (M&O) Contractor for the Mined Geologic Disposal System is studying the possibility of placing an underground repository to store high level nuclear waste at Yucca Mountain in Nevada. This nuclear waste will be placed in a waste package as shown in Figure 1.1 and then stored inside the repository. Therefore, the environment inside the repository has a major impact on the design of the waste package.

One of the repository's environmental factors is the amount of moisture that can flow though the repository's drift. The latest study of this environmental factor indicates a large increase of moisture flowing through the drifts for tens of thousands of years. Therefore, the current design of the waste package needs to be modified to protect the spent nuclear fuel from this excessive moisture. One of these modifications to the waste package design is coating the waste package with a material (Figure 1.2) that will help in keeping away the moisture from the spent nuclear fuel for the prescribed duration.

The ability to apply a coating on the waste package must first be determined to be possible. A literature search was performed to see if some other entity coats large cylindrical shapes. The results of this search indicate that the pulp and paper industry

uses thermal spray to coat the outside of their paper rollers. An example of this is a thermal sprayed refractory metallic coat on the Yankee dry rollers (1). Another is the plasma spraying of a nickel chromium alloy onto a coal-fired boiler tube (2). Finally, Caterpillar is developing a thick barrier coating for their diesel engine combustion chambers (3).

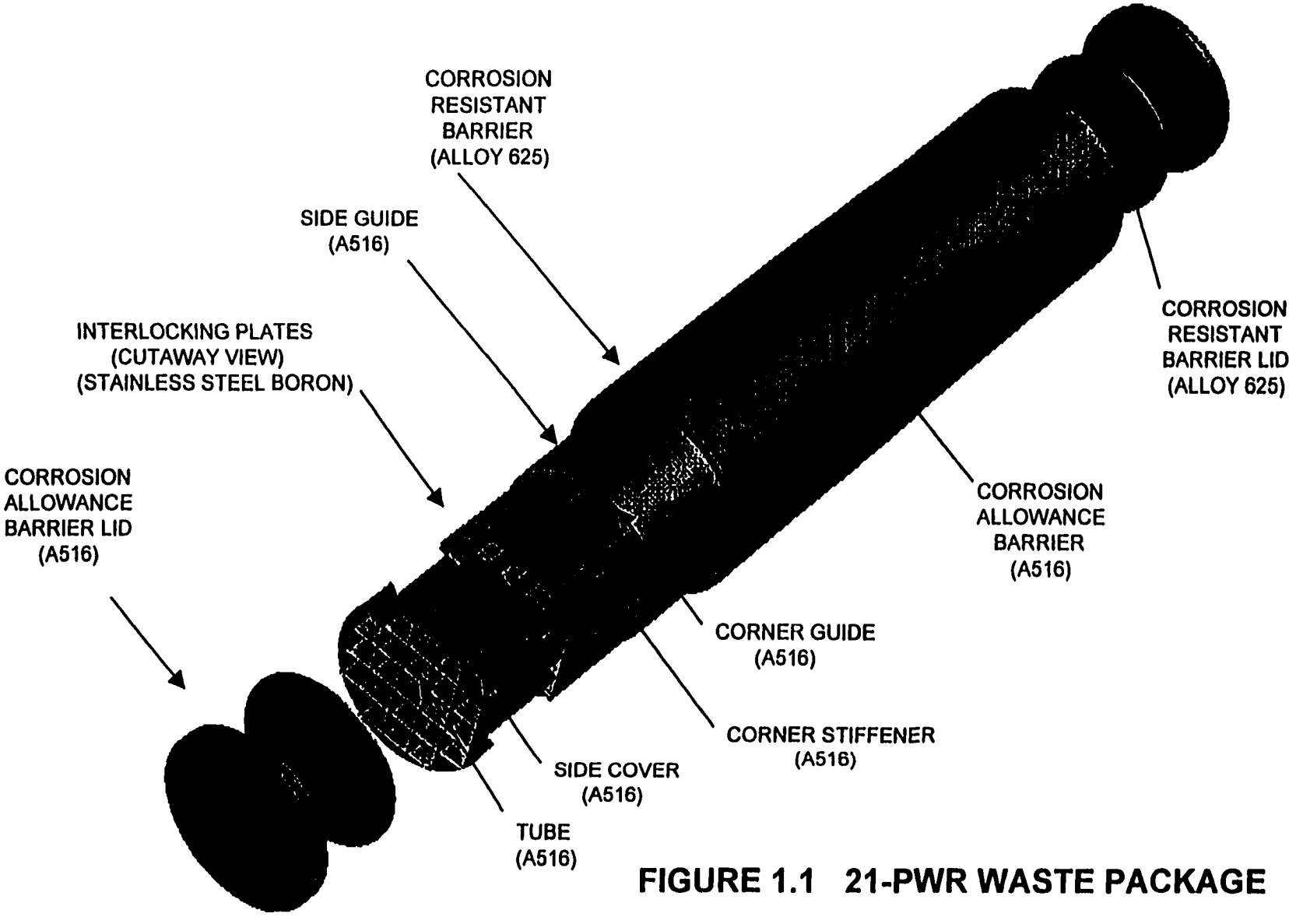

FIGURE 1.1 21-PWR WASTE PACKAGE

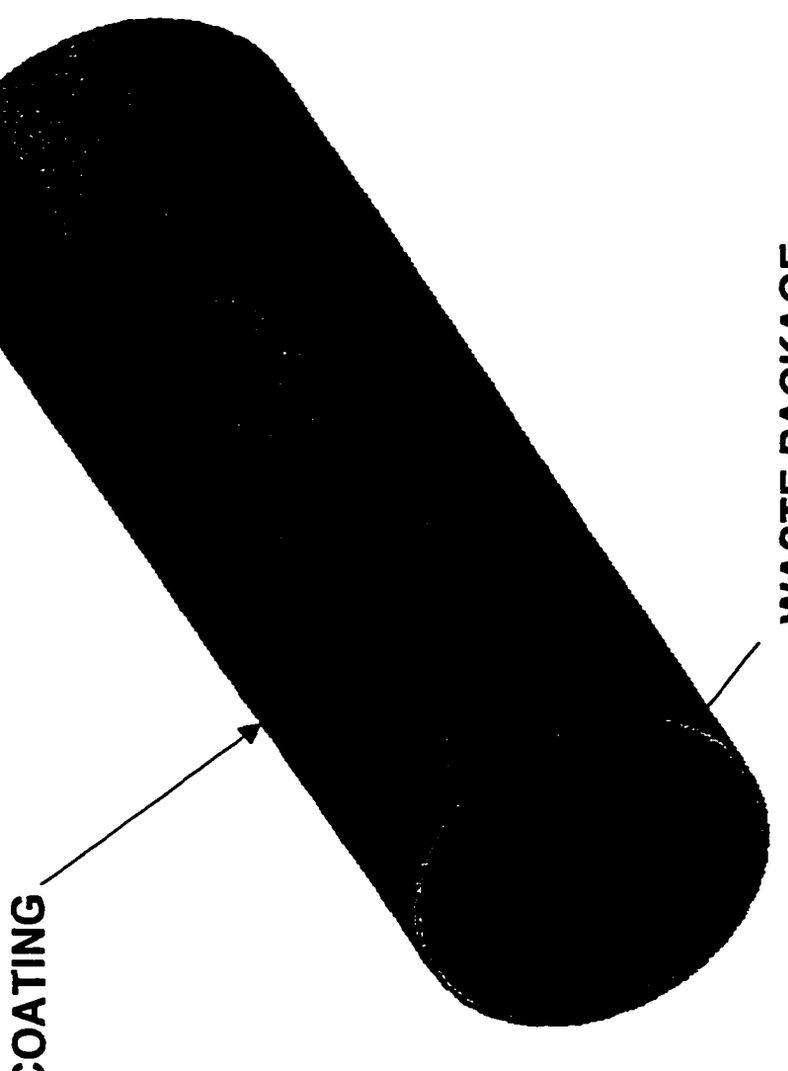

FIGURE 1.2 COATED WASTE PACKAGE

The purpose of this thesis is to answer some of the other questions concerning the feasibility of applying a thermal sprayed coating onto the waste package. The thesis is divided into four sections. The first section is composed of two chapters. These chapters describe the thermal spray process and three candidate thermal spray systems used to apply a coating onto a substrate. The next section describes the materials to be used as the coating materials. The third section studies the residual stress that is produced by the thermal spray process and compares two analysis methods to determine the accuracy of the residual stress. The final section of this thesis is an analysis of the thermal stress produced by the heat released from the spent nuclear fuel.

CHAPTER 2

THERMAL SPRAY PROCESS

The thermal spray process operates by taking a material in the form of rod, wire, or powder and heating this material into molten or semi-molten particles. After the heat up phase, the particles are then propelled from the thermal spray system to be impacted onto the material to be coated (substrate). These impinging particles may spread to form pancake-like splats (lamellae), or partially fragment into smaller droplets. The dynamic formation of a splat is a complex interplay of heat transfer and material flow as the particle's motion comes to rest, as shown in Figure 2.1

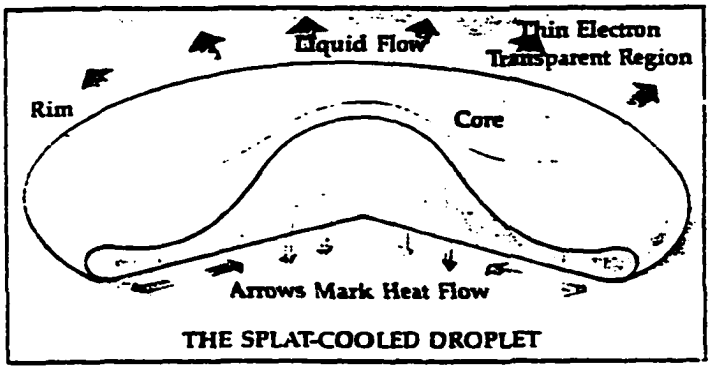

Figure 2.1 Model of a Splat as it Impacts Substrate (1)

The range sizes of typical lamellae are 1 to 5 μm thickness with a 50 to 100 μm diameter (4,5). The splats build a highly oriented structure on the substrate with the

lamellae parallel to the substrate surface. Finally, the integrity of the coating is dictated by the interactions of the splats with the substrate (adhesive strength) and with each other (cohesive strength).

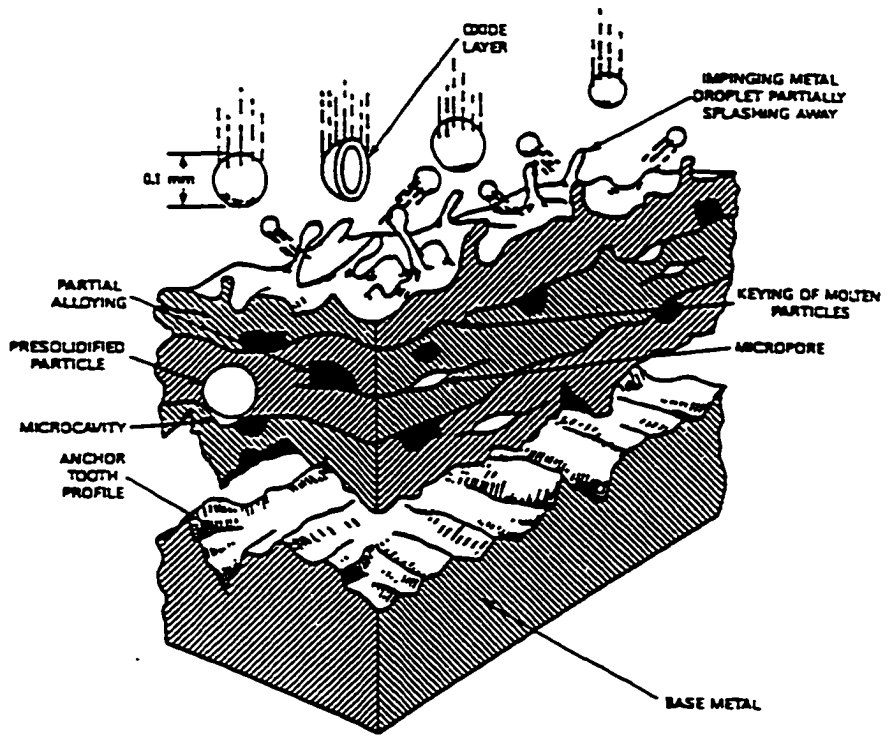

Figure 2.2 Generic Coating Structure (1)

Figure 2.2 depicts the typical features of the generic thermal spray coating. The impinging particle (if not an oxide to begin with) is likely to interact with the surrounding atmosphere during its time of flight, and entrapped oxide is often the demarcation of the boundary between splats. This boundary is also associated with significant porosity. In fact, recent work indicates that perhaps 20 to 30 percent of the interface between splats in a typical coating can be viewed as a microweld. The cohesion of the coating is, to some extent, derived from the interlocking fingers of the individual splats. Some of the

impinging particles may not be molten on impact, and this results in coating heterogeneity and additional porosity. The microstructure of the splat interior may itself be nonuniform. The brief residence time of the feed in the heating zone of the spray device may also result in undesirable coating heterogeneities that reflect nonuniformity of the feed itself. Figure 2.2 also suggests the importance of the surface profile of the substrate in determining the bond strength (1).

CHAPTER 3

THERMAL SPRAY SYSTEMS

INTRODUCTION

Thermal energy is derived in a thermal spray coating system by gas combustion or conversion of electrical energy. An example of gas combustion for heating the coating material is the "high-velocity oxy-fuel" (HVOF) system. Another gas combustion system is the detonation gun (D-gun) that uses discrete explosions to propel the coating material as well as heat it. The plasma spray system uses electrical energy to generate a high-temperature ionized gas. These thermal spray systems are shown schematically in Figures 3.1 through 3.3. These three methods are the candidates for applying a coating onto the waste package.

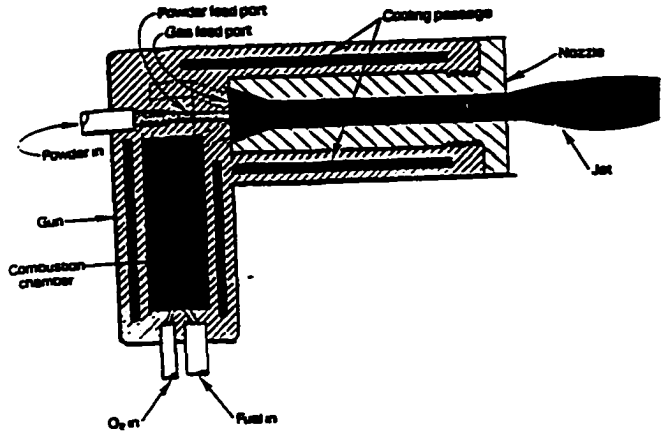

Figure 3.1 Schematic of the HVOF System (1)

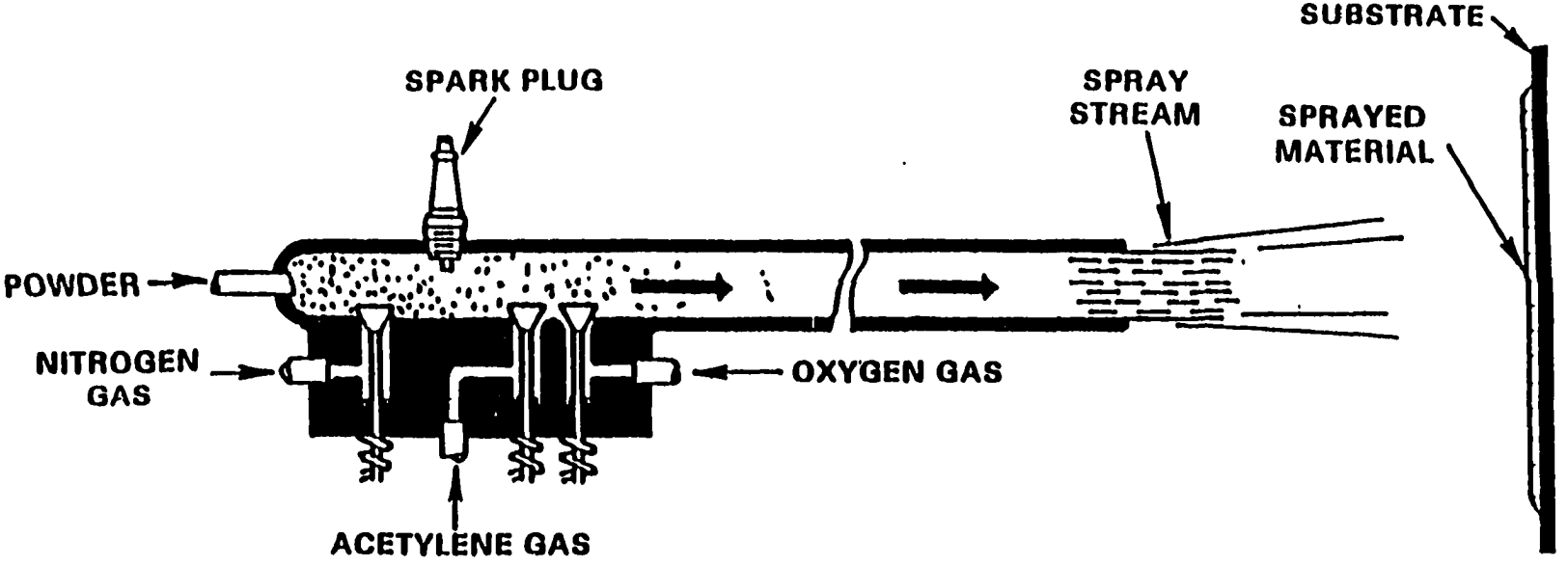

Figure 3.2 Schematic of Detonation Gun (6)

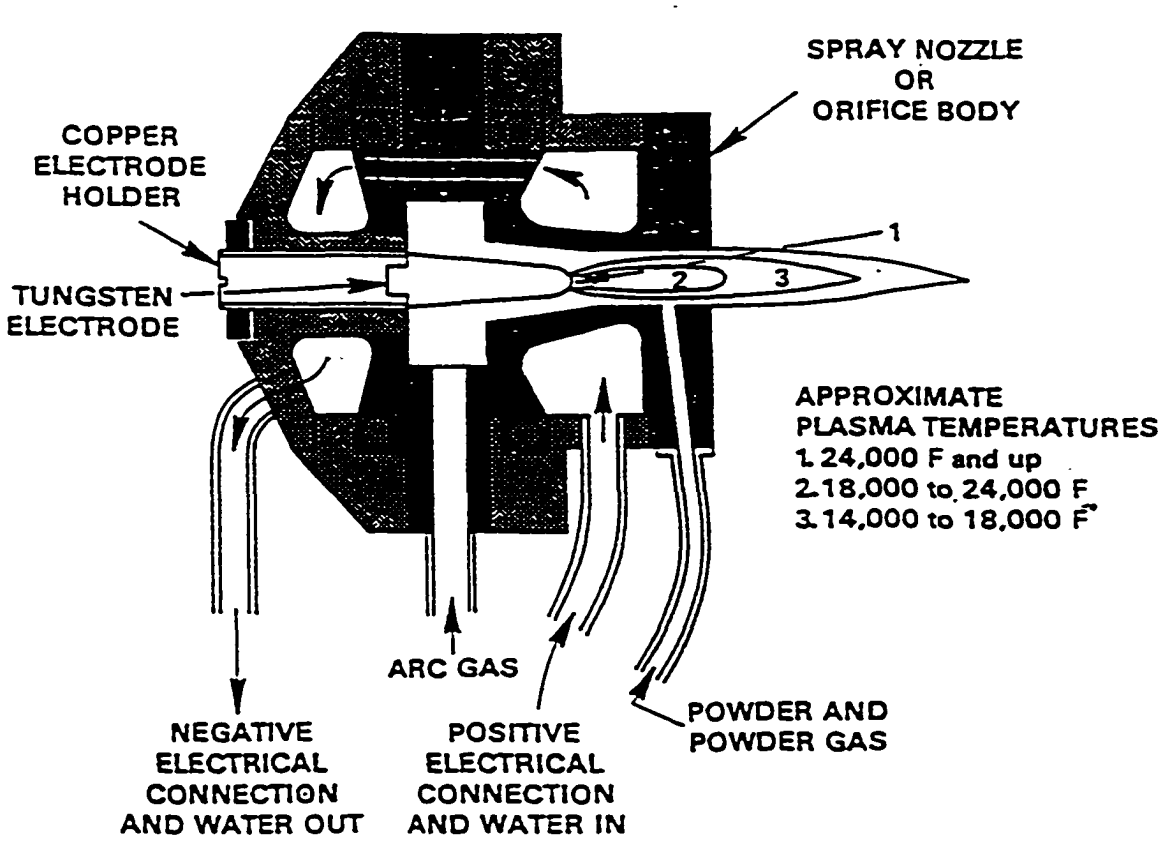

Figure 3.3 Cross Section of Typical Plasm-Spray Gun (6)

HIGH-VELOCITY OXY-FUEL SYSTEM

The HVOF system uses several processes to deliver a coating material onto a substrate. The process begins with a combustion of a fuel gas (propylene, hydrogen, or propane) that is injected under pressure with oxygen into a water-cooled combustion chamber. Next, the combustion gases are discharged through four ports in the combustion heads increasing gas velocity to hypersonic level and enabling the gas to make a 90 degree bend into a water-cooled nozzle. Another process is where the powder is injected via a carrier gas (nitrogen, argon, helium) into the intersection of the four exhaust gas streams, where the powder is evenly distributed into the core of the flame and propelled through the nozzle. Finally, the gas exits the nozzle at a hypersonic velocity, as indicated by the presence of visible shock diamonds in the flame.

These gas velocities have been measured in the range from 1,500 to 2,000 m/s, i.e. on order of five times the speed of sound (7). The flame temperature for this system is measured around 2900°C (8). This relatively low flame temperature makes it difficult to spray ceramics and refractory metals. Another difficulty is that this system requires the use of finer powder particle size and tighter particle distribution than other thermal spray systems. This difficulty is caused by the short dwell time for the particle in the flame that may not provide sufficient heat transfer to the large powder particles.

DETONATION GUN

The D-gun resembles a small cannon (9). Oxy-acetylene gas and powder are injected into the barrel and ignited with a spark plug. The combustion chamber is then flushed with nitrogen, and a new cycle begins (5). Operation frequency is typically four

to eight cycles per second, giving a relatively low spray rate of 0.3 to 0.9 kg/h (10). These discrete explosions generate noise on the order of 150 dB (5). This noise level is capable of causing "full body damage to the human ear," so acoustic isolation in a spray chamber is mandatory. The D-gun's spray velocity is estimated around 750 m/s (1).

PLASMA-SPRAYING

The conventional plasma-spraying process uses a DC arc between the tungsten alloy cathode and copper nozzle anode that heats a flowing inert gas stream, usually argon. This gas is partially ionized to make it into plasma. Some of the energy stored in the plasma flame is released when the gas "de-ionizes." Also, diatomic gases such as Nitrogen and Hydrogen are often added to the plasma gas to increase its enthalpy. These molecular bonds are broken when the gas is excited by the arc, and recombination of the atoms provides further energy for heating the feed material for the coating (5).

The combination of high temperature (17,000°C (11)), fast particle heating, and inert atmosphere of the plasma results in desirable coating characteristics for a broad range of spray materials (1). The particle velocity for 40 kW system is around 300 m/s and around 500 m/s for an 80 kW system (10).

CHAPTER 4

MATERIAL OPTIONS

INTRODUCTION

The materials that are used for the coating need to prevent moisture from contacting the spent nuclear fuel for tens of thousands of years. The reason for this requirement is to prevent the spent nuclear fuel from reaching criticality and releasing radionuclides to the general public. Therefore, three material classes are developed that might be used as a coating on the waste package. These classes are ceramics, metals, and functionally graded materials (FGMs).

CERAMICS

Ceramics have very high corrosion and high-temperature resistance, but with the disadvantages of being brittle and having relativity low tensile strength compared to metals. The two candidates from this group are alumina and zirconia-yittria. The reasons for choosing these two ceramics are their good corrosion resistant characteristic, the availability of their mechanical and thermal properties in literature, and their compatibility with the waste package materials like their thermal expansion coefficient values being as similar to carbon steel. The mechanical and thermal properties of these ceramics are given in Appendix A.

METALS

The metals in this class need to have better corrosion resistant properties than the waste package barriers that are made out of ASTM A516 carbon steel for the outer barrier and alloy 625 for the inner barrier. The candidate material for this class is alloy C-22. The selection of alloy C-22 is based on its high resistance to chloride ion stress-corrosion cracking; it also has excellent relative pitting resistance compared to many other nickel alloys and stainless steels. Alloy C-22 has superior tensile strength properties over other candidates from the ceramic class. The thermal and mechanical properties for alloy C-22 are listed in Appendix A.

FUNCTIONALLY GRADED MATERIALS

The FGMs material class use the same ceramic candidates as in the ceramic class, but also include a metallic component. The FGMs metallic part should be the same material as the waste package outer barrier, i.e. ASTM A516 carbon steel. FGMs are composed of various layers that can be predominantly metallic, ceramic, or an intermediate combination. Proper layering of these materials will lessen the stresses caused by the mismatches in the different coefficients of thermal expansion. The FGMs' mechanical and thermal properties are listed in Appendix A.

CHAPTER 5

RESIDUAL STRESS

INTRODUCTION

Residual stresses are caused by the thermal gradients produced during the manufacture of a component by welding, heat treating, and thermal spraying. An example of residual stress is when a uniformly heated part is quenched, the surface cools first. The subsequent thermal contraction of the core material is resisted by the outer skin, which is thereby placed in residual compression. The core is left in triaxial tension, following the rule "what cools last is in tension" (12).

The purpose of this chapter is to compare a one-dimensional mathematical model to a two-dimensional finite element analysis (FEA) model of the residual stresses at the interface between a substrate and coating at the time of thermal spraying process. This comparison is composed of three parts. The first part deals with determining the interface temperature during the thermal spray process. The second part is the determination of the residual stresses from this thermal spray process. Finally, the last part involves a comparison of these two models.

MATHEMATICAL MODEL

The mathematical model was developed by D. Stover, D. A. Jager, and H. G. Schutz (13) and was presented at the Fourth National Thermal Spray Conference held in Pittsburgh, PA. This model is based on experimental data to develop the interface temperature equation and the residual stress equation.

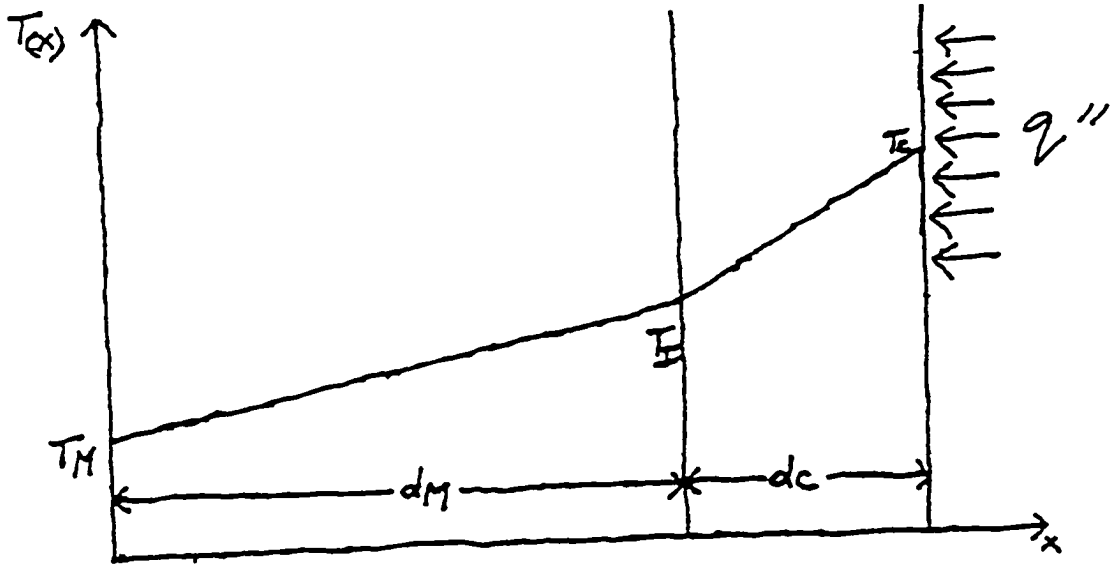

Figure 5.1 Steady State Temperature Distribution During Spraying

Figure 5.1 shows the steady state temperature distribution during thermal spraying, and where C is the coating and M is the metal substrate. The steady state temperature distribution is based on a constant heat flux from the spraying process that creates a steady state temperature field with a constant gradient of temperature across the substrate and the coating. From this diagram the steady state heat conduction equation is derived; by using differential equations the equation for the interface temperature is developed. This process is described on the next page.

Steady state heat conduction equation:

$$\frac{d^2T}{dx^2}=0 \tag{5.1}$$

$$q''=-k\frac{dT}{dx} \tag{5.2}$$

Boundary Conditions:

$$T(0)=T_M \tag{5.3}$$

$$T_M(d_M)=T_C(d_M) \tag{5.4}$$

$$-k_M\frac{dT_M}{dx}\Big|_{x=d_M}=-k_C\frac{dT_C}{dx}\Big|_{x=d_M} \tag{5.5}$$

$$-k_C\frac{dT_C}{dx}\Big|_{x=d_M+d_C}+q''=0 \tag{5.6}$$

Analytical Solution:

$$T_M(x)=\frac{q''}{k_M}x+T_M \tag{5.7}$$

$$T_C(x)=\frac{q''}{k_M}[x+d_M(\frac{k_C}{k_M}-1)]+T_M \tag{5.8}$$

Temperature at the interface:

$$T_I=\frac{q''}{k_M}d_M+T_M \tag{5.9}$$

where q" = heat flux (W/m^2), k_M = thermal conductivity of the metal (W/mK), k_C = thermal conductivity of the coating (W/mK), T_M = temperature of the metal (K), T_C = temperature of the coating (K), T_I = temperature of the interface (K), d_M = distance of the metal (m), and d_C = distance of the coating (m).

The interface temperature during the thermal spray process for the waste package's coating used the following values:

$q" = 1x10^6$ W/m^2 (13)

$k_M = 40.84$ W/mK

$T_M = 298.15$ K (25 °C)

$d_M = .1$ m

The interface temperature is 2,747 K (2,474 °C) by applying the above values. This interface temperature is used for the alumina, zirconia-yttria, and C-22 alloy cases. Thus the interface temperature is not based on any coating material values - only the heat flux input and the metal substrate's properties.

The residual stress equation is developed for a thin oxide coating on an infinite plane. This equation is shown below (13):

$$\sigma_R = \frac{E_C}{1-\upsilon_C}(\alpha_M - \alpha_C)(T - T_I) \qquad (5.10)$$

where E_C = Young's modulus of the coating (Pa), ν_C = Poisson's ratio of the coating, α_M = Thermal expansion coefficient of the metal ($°C^{-1}$), α_C = Thermal expansion coefficient of the coating ($°C^{-1}$), T = temperature at which the stress is measured (°C) (normally ambient temperature), T_I = interface temperature (°C), and σ_R = residual stress (Pa).

The residual stress for the three coating materials was calculated using Equation 3.10. The residual stress for alumina is -165 MPa, for zirconia-yttria is -322 MPa, and -487 MPa for C-22 alloy. These residual stresses are so small as to be considered negligible.

FINITE ELEMENT ANALYSIS

The ANSYS finite element analysis (FEA) code was used to find the residual stress at the interface between the coating and the substrate. The ANSYS FEA code is chosen to solve for residual stress because it is one of the better commercial codes and is accepted by the Nuclear Regulatory Commission to perform structural and thermal analyses.

The governing equations for the residual stress are based on heat flow fundamentals and the principle of virtual work. The thermal section of the residual stress analysis uses the first law of thermodynamics and Fourier's second law. These equations are shown below:

$$\rho c\left(\frac{\partial T}{\partial t}[v]^T[L]T\right)+[L]^T[q]=q''' \qquad (5.11)$$

where ρ = density, c = specific heat, T = temperature, t = time, [L] = partial derivative vector operator, [v] = velocity vector for mass transport of heat, [q] = heat flux vector, and q''' = heat generation rate per unit volume.

$$[q] = \begin{bmatrix} k_{xx} & 0 & 0 \\ 0 & k_{yy} & 0 \\ 0 & 0 & k_{zz} \end{bmatrix} [L]T \tag{5.12}$$

where k_{xx}, k_{yy}, k_{zz} = thermal conductivity in the element x, y, and z directions, respectively.

Equations 5.11 and 5.12 are combined to form the Equation 5.13 to solve for temperature, as shown below:

$$\rho c\left(\frac{\partial T}{\partial t} + v_x\frac{\partial T}{\partial x} + v_y\frac{\partial T}{\partial y} + v_z\frac{\partial T}{\partial z}\right) = q''' + \frac{\partial}{\partial x}\left(k_x\frac{\partial T}{\partial x}\right) + \frac{\partial}{\partial y}\left(k_y\frac{\partial T}{\partial y}\right) + \frac{\partial}{\partial z}\left(k_z\frac{\partial T}{\partial z}\right) \tag{5.13}$$

The structural section of the residual stress analysis uses virtual work that states a very small change of the internal strain energy must be offset by an identical change in external work due to the applied loads, or:

$$\delta U = \delta V \tag{5.14}$$

where U = strain energy (internal work) = $U_1 + U_2$, V = external work = $V_1 + V_2 + V_3$, and δ = virtual operator. The virtual Strain Energy is:

$$\delta U_1 = \int_{vol} [\delta\varepsilon]^T [\sigma] d(vol) \tag{5.15}$$

where [ϵ] = strain tensor, [σ] = stress tensor, and vol = volume of element. Continuing the derivation assuming linear materials and geometry, Equation 5.14 and Equation 5.15 are combined to give:

$$\delta U_1 = \int_{vol} ([\delta\varepsilon]^T[D][\epsilon] - [\delta\varepsilon]^T[D][\epsilon^{th}])d(vol) \tag{5.16}$$

where [D] = elasticity matrix and [ϵ^{th}] = thermal strain tensor. The strains may be related to the nodal displacement by:

$$[\epsilon] = [B][u] \tag{5.17}$$

where [B] = strain-displacement matrix, based on the element shape functions and [u] = nodal displacement vector. It will be assumed that all effects are in the global Cartesian system. Combining Equations 5.16 and 5.17, and noting that the nodal displacement vector does not vary over the volume:

$$\delta U_1 = [\delta u]^T \int_{vol} [B]^T[D][B]d(vol)[u] - [\delta u]^T \int_{vol} [B]^T[D][\varepsilon^{th}]d(vol) \tag{5.18}$$

Another form of virtual strain energy is when a surface moves against a distributed resistance, as in a foundation stiffness. This may be written as:

$$\delta U_2 = \int_{area_f} [\delta w_n]^T[\sigma]d(area_f) \tag{5.19}$$

where [w_n] = motion normal to the surface vector, [σ] = stress carried by the surface vector, and $area_f$ = area of the distributed resistance. Both the motion normal to the surface vector and the stress carried by the surface vector will usually have only one non-zero component. The point-wise normal displacement is related to the nodal displacement by:

$$[w_n] = [N_n][u] \tag{5.20}$$

where $[N_n]$ = matrix of shape functions for normal motions at the surface. The stress, $[\sigma]$, is

$$[\sigma] = k[w_n] \tag{5.21}$$

where k = the foundation stiffness in units of force per length per unit area. Combining Equations 5.19, 5.20, and 5.21, and assuming k is constant over area:

$$\delta U_2 = [\delta u]^T k \int_{area_f} [N_n]^T [N_n] d(area_f)[u] \tag{5.22}$$

Next, the external virtual work will be considered. The inertial effect is developed first:

$$\delta V_1 = -\int_{vol} [\delta w]^T \frac{[F^a]}{vol} d(vol) \tag{5.23}$$

where [w] = vector of displacements of a general point, and $[F^a]$ = acceleration (D'Alembert) force vector. According to Newton's second law:

$$\frac{[F^a]}{vol} = \rho \frac{\partial^2}{\partial t_2}[w] \tag{5.24}$$

where ρ = density and t = time. The displacements within the element are related to the nodal displacements by:

$$[w] = [N][u] \tag{5.25}$$

where [N] = matrix of shape functions. Combining Equation 5.23, Equation 5.24, and Equation 5.25 and assuming that density is constant over the volume:

$$\delta V_1 = -[\delta]^T \rho \int_{vol} [N]^T [N] d(vol) \frac{\partial^2}{\partial t^2} [u] \tag{5.26}$$

The pressure force vector formulation starts with:

$$\delta V_2 = \int_{area_p} [w_n]^T [P] d(area_p) \tag{5.27}$$

where [P] = the applied pressure vector (normally contains only one non-zero component) and $area_p$ = area over which pressure acts. Combining Equations 5.25 and 5.27:

$$\delta V_2 = [\partial u]^T \int_{area_p} [N_n]^T [P] d(area_p) \tag{5.28}$$

Unless otherwise noted, pressures are applied to the outside surface of each element and are normal to curved surfaces, if applicable. Nodal forces applied to the element can be accounted for by:

$$\delta V_3 = [\delta u]^T [F^{nd}_e] \tag{5.29}$$

where $[F^{nd}_e]$ = nodal forces applied to the element vector. All material properties for stress analysis elements are evaluated at the average temperature of each element. Finally, Equations 5.14, 5.18, 5.22, 5.26, 5.28, and 5.29 may be combined to give:

$$[\delta u]^T \int_{vol} [B]^T [D][B] d(vol)[u] - [\delta u]^T \int_{vol} [B]^T [D][\varepsilon^{th}] d(vol) \tag{5.30}$$

$$+[\delta u]^T k \int_{area_f} [N_n]^T [N_n] d(area_f)[u]]$$

$$= -[\delta]^T \rho \int_{vol} [N]^T [N] d(vol) \frac{\partial^2}{\partial t^2}[u] + [\partial u]^T \int_{area_p} [N_n]^T [P] d(area_p) + [\delta u]^T [F^{nd}_e]$$

Noting that the $[\delta u]^T$ vector is a set of arbitrary virtual displacements common in all of the above terms, the condition required to satisfy Equation 5.30 reduces to:

$$([K_e] + [K^f_e])[u] - [F^{th}_e] = [M_e][u''] + [F^{pr}_e] + [F^{nd}_e] \tag{5.31}$$

where $[Ke] = \int_{vol} [B]^T[D][B]d(vol)$ = element stiffness matrix, $[K^f_e] = k\int_{areaf} [N_n]^T[N_n]d(area_f)$ = element foundation stiffness matrix, $[F^{th}_e] = \int_{vol}[B]^T[D][\epsilon^{th}]d(vol)$ = element thermal load vector, $[M_e] = \rho\int_{vol}[N]^T[N]d(vol)$ = element mass matrix, $[u''] = \partial^2/\partial t^2[u]$ = acceleration vector, and $[F^{pr}_e] = \int_{areap} [N_n]^T[P]d(area_p)$ = element pressure vector. The theory on how the ANSYS finite element code solves thermal and structural problems is given in Appendix B.

A one-dimensional steady state model is used in the FEA. The reason for using this type of model for the FEA is to compare the FEA model to the one-dimensional mathematical model. Further FEA work could be performed with a three-dimensional transient dynamic model to help understand localized stresses.

The FEA of the residual stress of alumina, zirconia-yttria, and C-22 alloy employs a multiple step process. The first step of this process is to develop a one-dimensional model of the waste package with a 5 mm layer of coated material made out of plane

elements. Each element has four nodes with a single degree of freedom, temperature, at each node. This model is shown in Figure 5.2. After the model schematic is developed then a heat flux of $1x10^6$ W/m^2 is applied to the coating's elements and the temperatures are found. Next, the elements are changed to plane elements where each element is defined by four nodes having two degrees of freedom; translations in the nodal x direction and y directions. The temperatures from the heat transfer analysis are used to analyze the residual stress caused by the coating process. Finally, the radial stress values at the nodes that define the interface region are compared to the allowable stresses of the coating and the metal substrate for each case.

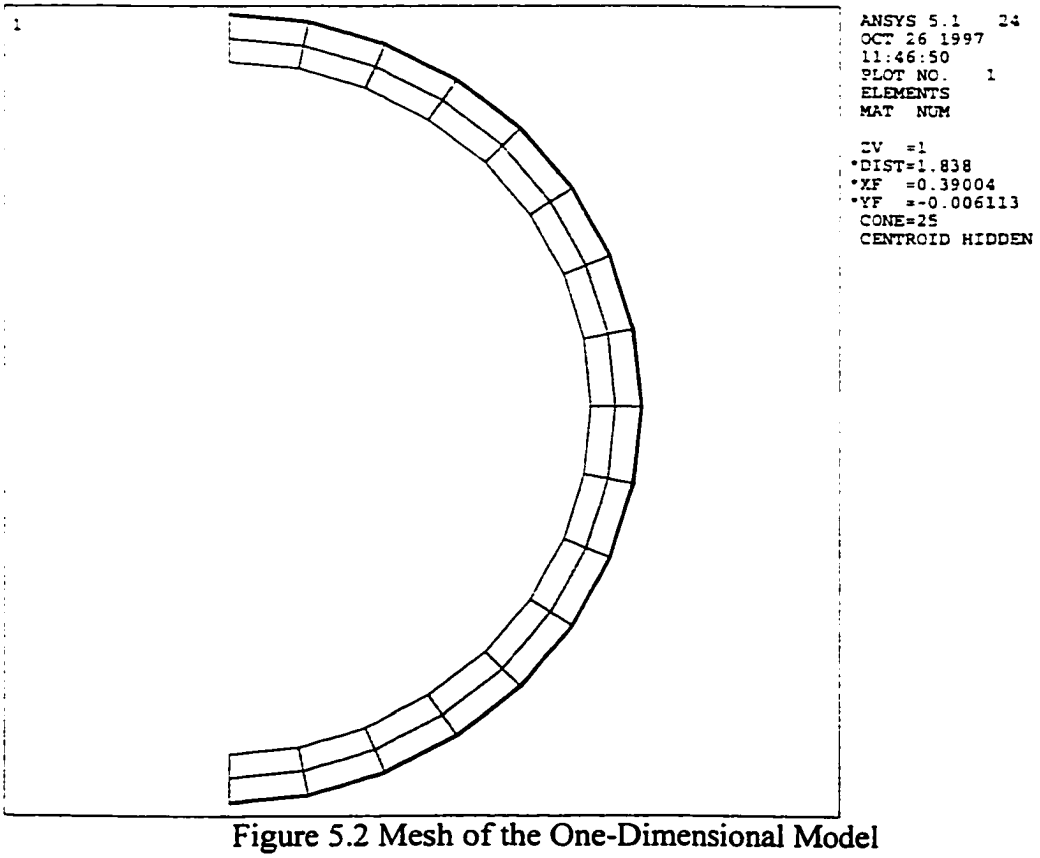

Figure 5.2 Mesh of the One-Dimensional Model

The results for this FEA process have two parts. The first part is the interface temperature value. All three cases have the same interface temperature value of 2,636°C (Figure 5.3). The next result is the residual stress values for the fifteen nodes that define the interface region; these values are listed in Table 5.1 (Figures 5.4 through 5.6). The residual stress values are below the compressive and tensile strength values for the given coating and the metal substrate.

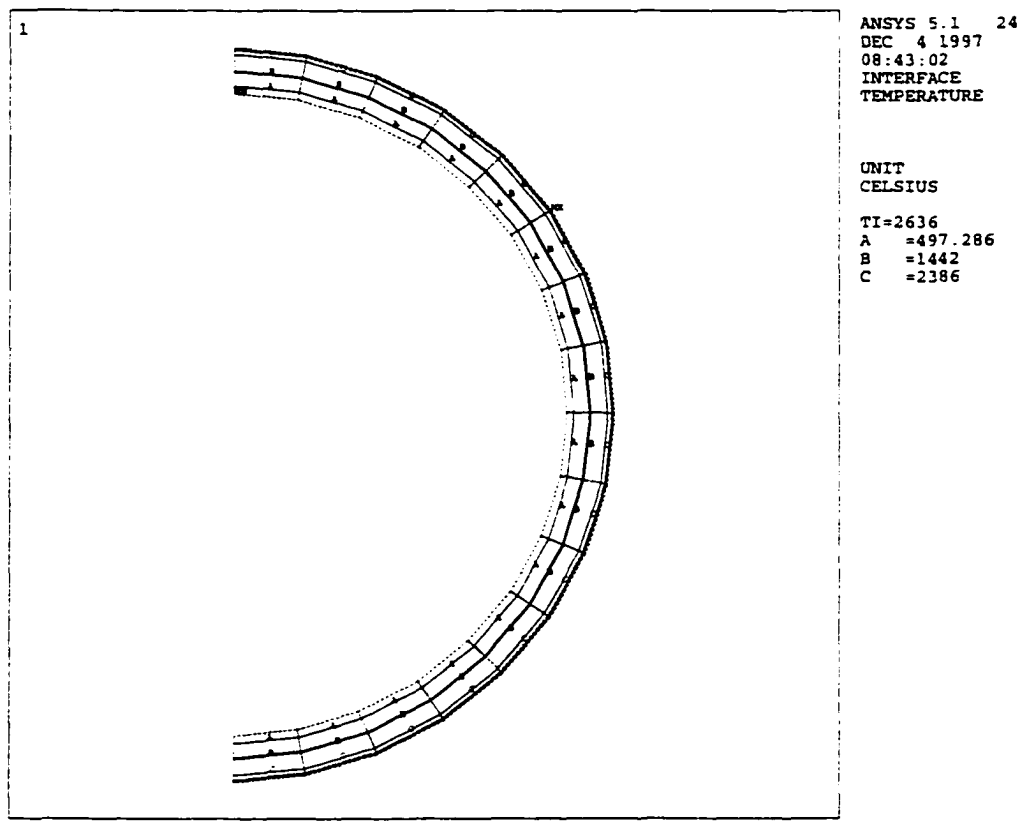

Figure 5.3 Temperature Profile

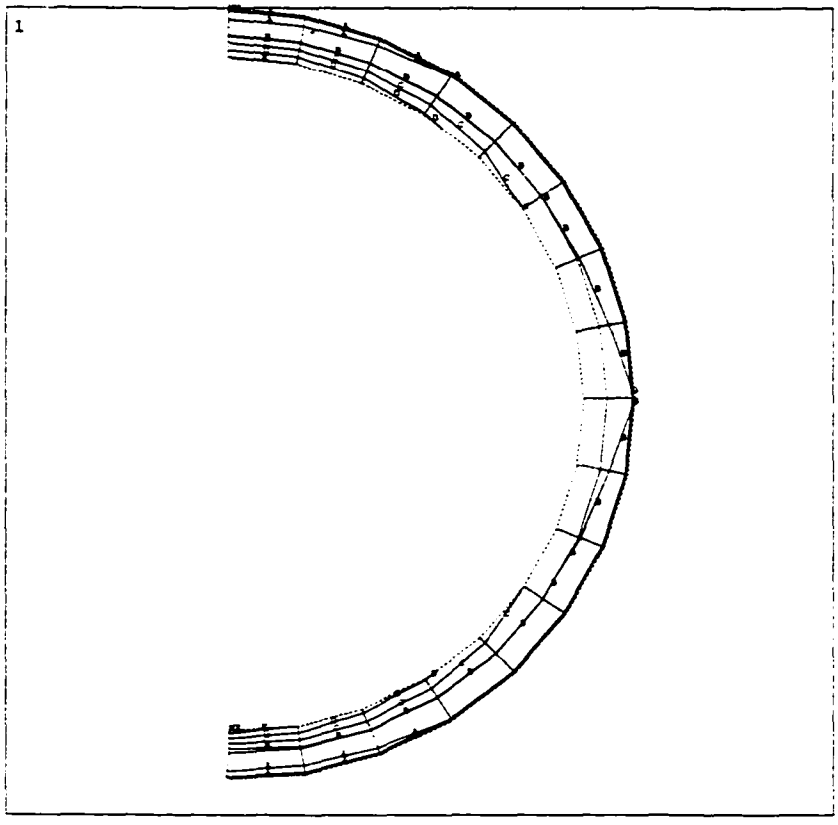

Figure 5.4 Stress Profile of the Alumina Case

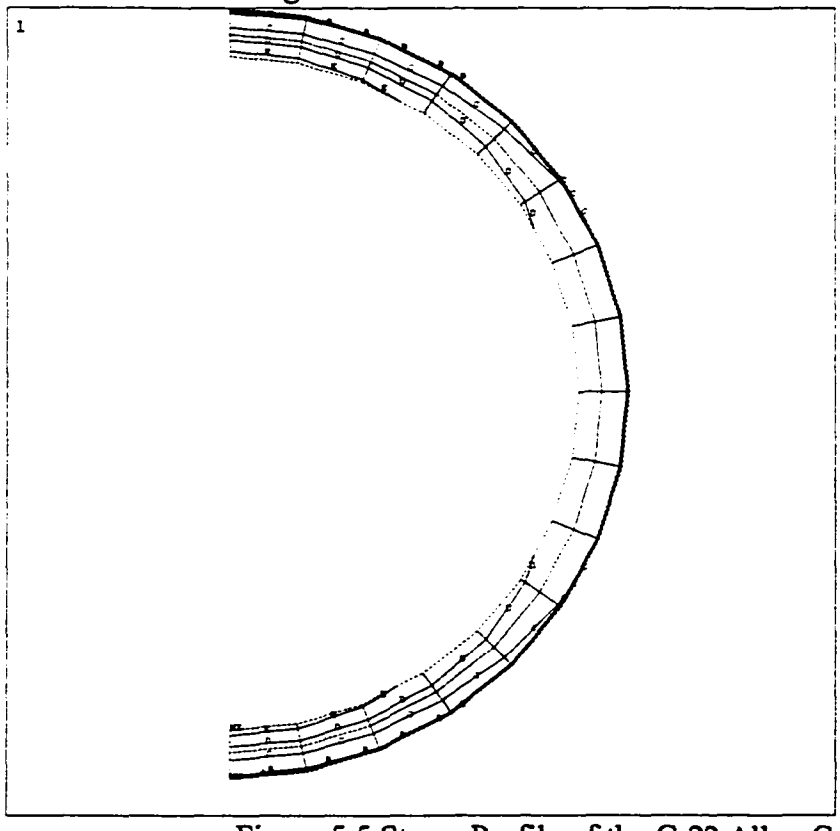

Figure 5.5 Stress Profile of the C-22 Alloy Case

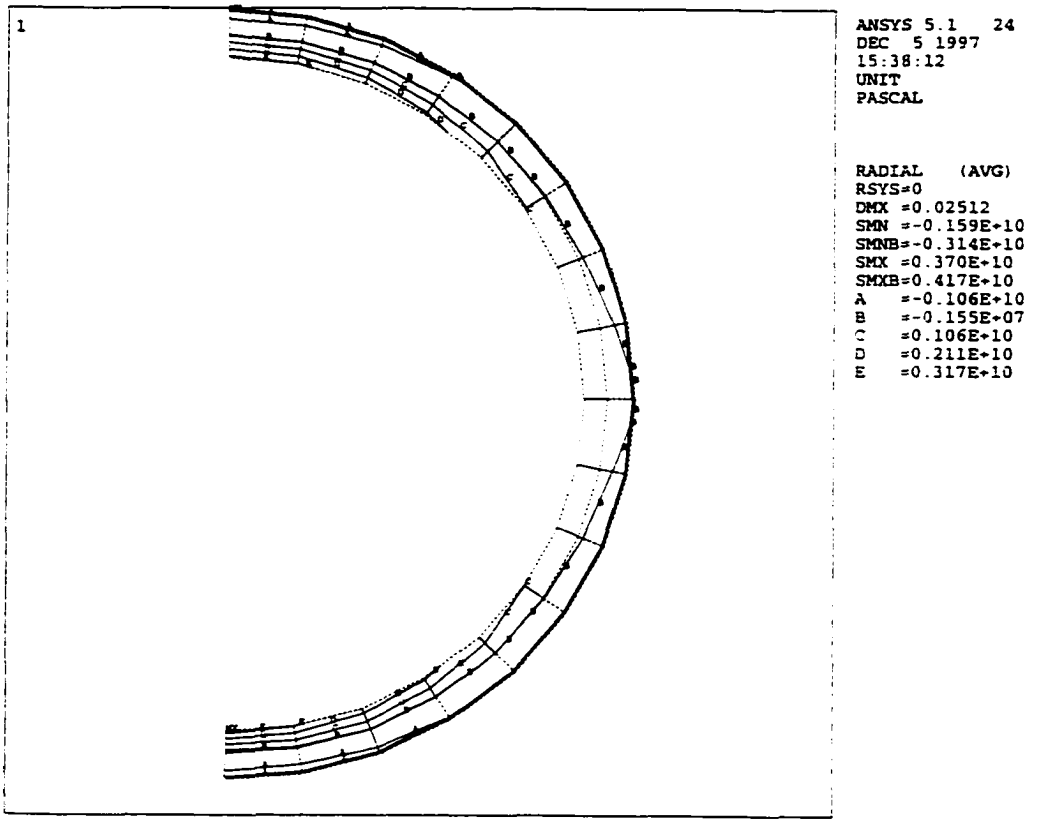

Figure 5.6 Stress Profile of the Zirconia-Yttria Case

Table 5.1 Residual Stress at the Interface Region of the FEA

Node Number	Alumina (MPa)	Zirconia-Yttria (MPa)	C-22 Alloy (MPa)
1	-77.7	67.0	-2800
8	-75.5	-65.7	-2690
12	-34.1	-27.7	-1400
13	-55.6	-482	-1940
18	-0.0893	4.34	-402
19	-34.1	-27.2	-880
24	22.3	28.1	26.1
25	-19.6	-20.4	-143
30	22.7	35.8	-357
31	-33.3	-36.6	-167
36	8.16	21.4	-1330
37	-63.1	-65.5	-936
42	-19.3	-3.67	-2340
43	-85.6	-82.3	-1980
47	-127	-127	-2770

COMPARISONS

There are two values that need to be compared from the mathematical model and FEA model for each case analyzed for residual stress at the interface. The interface temperatures of each method are compared. The interface temperature for the mathematical model is 2474°C and the interface temperature for the FEA model is 2636°C. The comparison of these two values produces a percent difference of 6.5% (Appendix C). This percent difference value indicates that both methods are compatible with each other to produce the same interface temperature value.

The next comparison is the residual stress value between these two methods. This comparison is based on the mathematical residual stress value and the average residual stress value of the interface region nodes. The alumina mathematical model has a residual stress of -165 MPa and the alumina FEA model has an average residual stress value of -38.1 MPa. The percent difference between these two methods is 76.9%. The zirconia-yttria mathematical model has a residual stress of -322 MPa and the zirconia-yttria FEA model has an average residual stress value of -61.0 MPa. The percent difference between these two methods is 81.1%. Finally, the C-22 alloy mathematical model has a residual stress of -487 MPa and the C-22 alloy FEA model has an average residual stress value of -1340 MPa. The percent difference between these two methods is 175%.

There are several reasons for the high percent difference between the two methods to find residual stress at the interface. One reason for the high percent difference is the difference in geometry between the two methods. The geometry used for the mathematical model is based on a one-dimensional infinite plane, but the FEA model geometry uses a one-dimensional semicircular shape. Another difference is the amount of constraint employed for each method. There is a one-dimensional constraint for the mathematical model to define an infinite plane. The constraints for the FEA model are used to encompass symmetry in the horizontal direction, and apply gravity at the bottom end of the waste package. A third difference is that the mathematical model is a steady state analysis and the FEA model is a dynamic analysis. These differences between the two methods would cause high percent difference between them. Therefore, the mathematical method can be used as a simple method to find the residual stress for the

thermal spray process, while the FEA method is best used for a more detailed answer for a residual stress value.

CHAPTER 6

THERMAL STRESS

INTRODUCTION

The purpose of this analysis is to determine whether the thermal stress caused by the heat output of the spent nuclear fuel being placed into the waste package will cause enough deformation to spall the coating from the waste package's corrosion allowance barrier. This chapter will discuss the development of the variable heat flux across the length of the waste package that is applied to the ANSYS's FEA model. The next section will discuss the thermal analysis portion of the thermal stress analysis, followed by a section which discusses the stress from the thermal analysis. Finally, the results of the thermal stress analysis cases and the conclusion of these results are presented.

VARIABLE HEAT FLUX DEVELOPMENT

The heat flux from the spent nuclear fuel is produced from the decay heat of the fission products. The steady state equation to calculate the standard heat flux produced by all the spent nuclear fuel assemblies in a waste package described below:

$$q'' = \frac{qN}{\pi LD} \tag{6.1}$$

nuclear fuel assembly (m), and D = inner diameter of the corrosion resistant barrier of the waste package (m).

The calculation to find this heat flux is based on a 21 pressurized water reactor waste package, as shown in Figure 1.1, with an inner diameter of the corrosion resistant barrier of 1.4234 m. The spent nuclear fuel assembly has a length of approximately 4 m and a heat transfer rate of 850.01 W/assembly (14,15) based on ninety percent of the pressurized water reactor spent nuclear fuel waste stream. These inputs give a heat flux of 997.95 W/m^2.

The development of the variable heat flux across the length of the spent nuclear fuel assembly uses a standard heat flux that is calculated from Equation 6.1. This value is multiplied by the relative value of a certain elevation from the predicted decay heat curve from Figure 6.1. The results of these heat fluxes are shown in Table 6.1

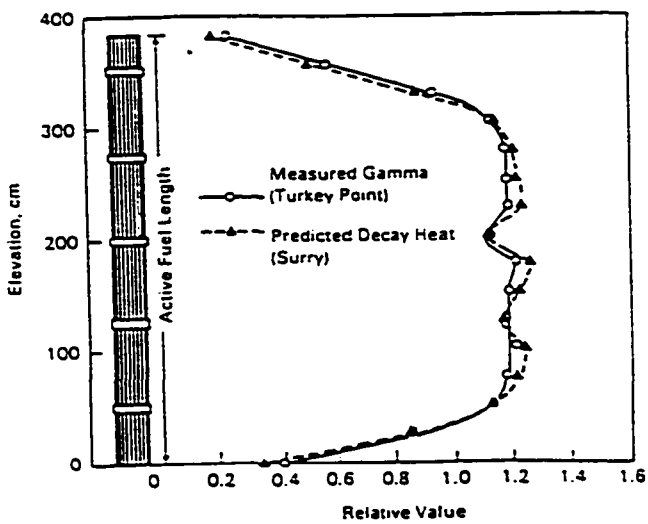

Figure 6.1 Predicted Axial Decay Heat Profile (14)

Table 6.1 Heat Fluxes Across Spent Nuclear Fuel Assembly

Elevation (m)	Relative Value	Heat Flux (W/m^2)
0 - 0.5	0.3	299.38
0.5 - 1.0	1.10	1097.74
1.0 - 1.5	1.21	1207.51
1.5 - 2.0	1.21	1207.51
2.0 - 2.5	1.12	1117.70
2.5 - 3.0	1.25	1247.43
3.0 - 3.5	1.15	1147.64
3.5 - 4.0	0.6	598.77

THERMAL ANALYSIS

The first step in performing a finite element analysis is the development and meshing of the model. The problem domain consists of a three-dimensional model of the corrosion allowance barrier and 5 mm thick coating as shown in Figure 6.2. The total length of the corrosion allowance barrier is 5.335 m with two skirts 0.225 m in length and 0.6 m thickness; the inner diameter of the corrosion allowance barrier is 1.4634 m, and the outer diameter is 1.6634 m. Symmetry is used in the model by cutting the waste package in half along its length. The model is composed of three-dimensional eight nodal elements with a single degree of freedom, temperature at each node.

There is a difference between the ceramic and metal models and the FGMs models. This difference is in the coating section; the ceramic and metal models are composed of one material element while the FGMs models are composed of four material elements. The reason for this difference is to show the grading of materials across the

coating.

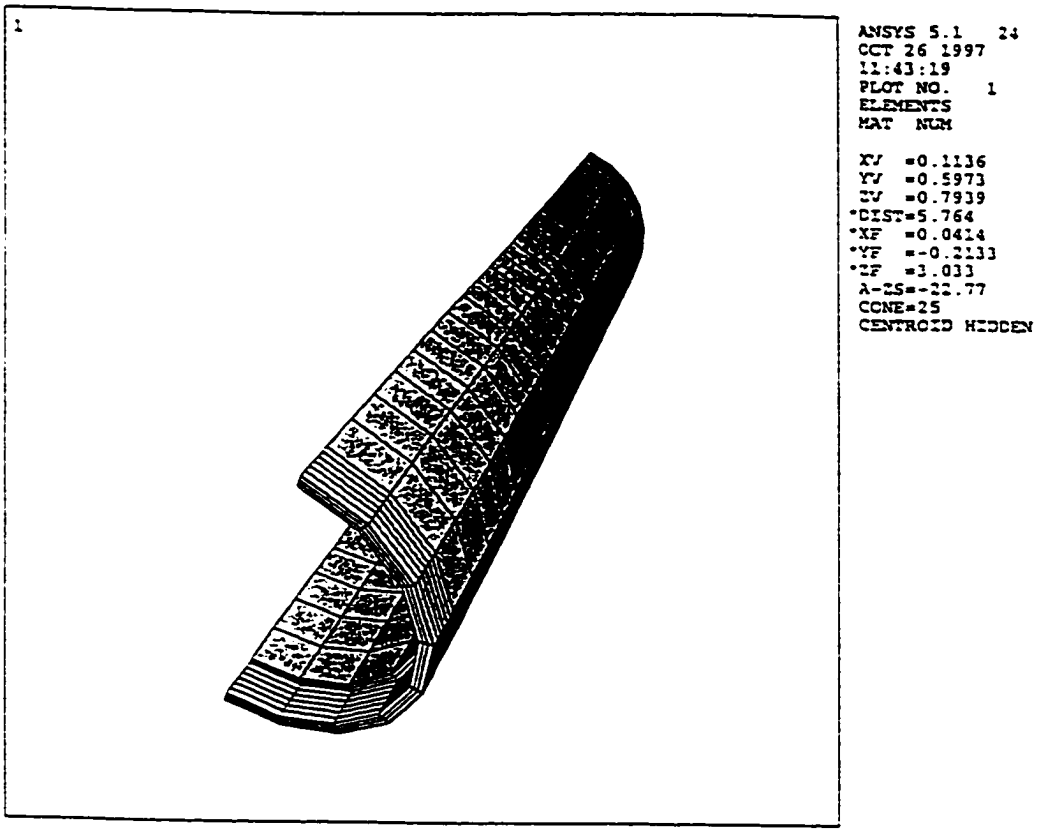

Figure 6.2 Mesh of Thermal Stress Model

After a specific model has been developed, the temperature boundary conditions are applied to the outer layer of the coating that does not take account of radiation heat transfer because radiation heat transfer does not have a effect in this thermal stress analysis as shown in Appendix C. This temperature boundary condition is 25°C, based on the fact the spent nuclear fuel is being loaded into the waste package at room temperature. Next, the heat fluxes are applied using values from Table 6.1 on the top, middle and bottom of the inside cavity of the waste package. Finally, the model is solved by the ANSYS package (Appendix B) that uses the Equation 3.11 through 3.13. The results of the thermal analysis are given in the results section of this chapter.

STRESS ANALYSIS

The stress analysis uses the same mesh model that was developed for the thermal analysis except that the elements are changed to elements that are three-dimensional eight nodal elements and each node has three degrees of freedom. The degrees of freedoms are the translations in the nodal x, y, and z directions. Also, the stress analysis uses the resultant temperatures produced from the thermal analysis as the load. The boundary conditions for the stress analysis are that the top and bottom ends of the waste package. The ends allow no movement in the x direction and the bottom end also allows no movement in the y direction; the bottom front node allows no movement in the z direction. Next, the model is solved using the ANSYS solver that uses the Equation 3.14 through Equation 3.31.

The resultant stresses are given as the first and third principal stress values and are given in the results section of this chapter. The principal stresses are used to describe the

maximum and minimum stress values of an object that experiences a load. These values are not dependent of the type or the placement of the coordinate system used to describe the location of the object. The first principal stress value is the maximum stress value and the third principal stress value is the minimum stress value. The subtraction of the third principal stress from the first principal stress and divided this result by two gives the maximum shear stress.

RESULTS

The maximum temperatures from the thermal analysis for the ceramic materials are 26.92°C for alumina (Figure 6.3) and 27.81°C for zirconia-yttria (Figure 6.4). The maximum total displacement from the thermal stress analysis is 4.68×10^{-5} m for alumina (Figure 6.5) and 6.77×10^{-5} m for zirconia-yttria (Figure 6.6). The maximum tensile and compressive stresses from these analyses are the first and third principal stresses, respectively. The values for the first principal stresses are 0.329 MPa for alumina (Figure 6.7) and 0.906 MPa for zirconia-yttria (Figure 6.8) and the third principal stresses are -0.563 MPa for alumina (Figure 6.9) and -0.742 MPa for zirconia-yttria (Figure 6.10). These stresses do not exceed the compressive strength and tensile strength of the alumina and the zirconia-yttria and adhesive strength (strength to maintain the bond between the substrate and coating) of the interface. The maximum shear stress values are 0.446 MPa for alumina and 0.824 MPa for zirconia-yttria. These stresses do not exceed half the adhesive strength value of the interface. Hence, the thermal stress from the spent nuclear fuel being placed in an alumina or zirconia-yttria coated waste package has no impact on the bond between the coating and the waste package corrosion allowance barrier.

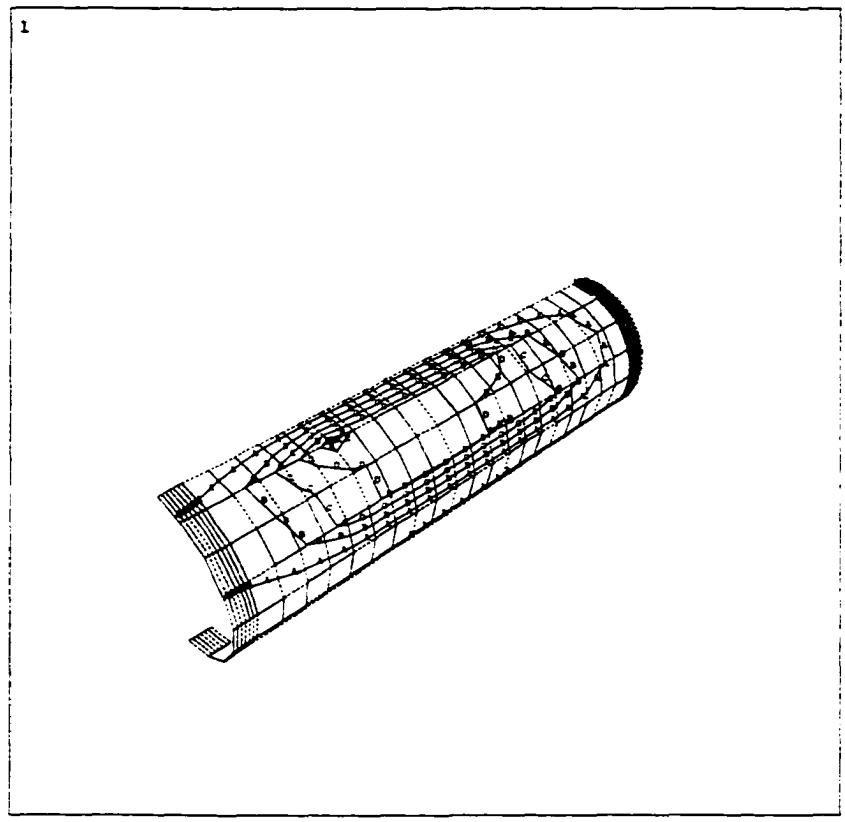

Figure 6.3 Temperature Profile of the Alumina Case

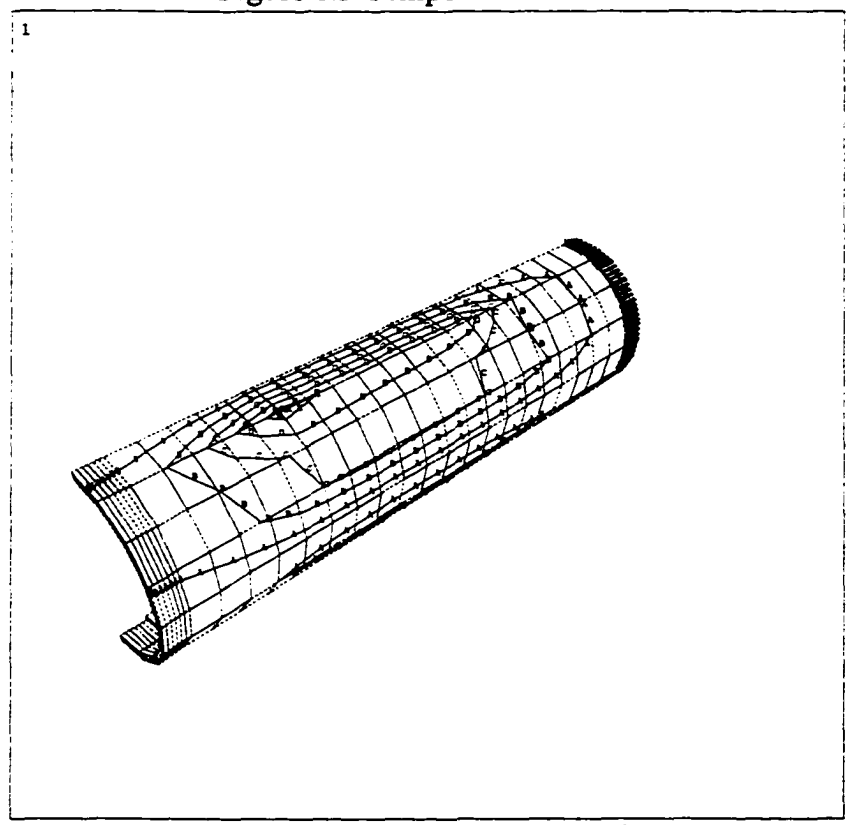

Figure 6.4 Temperature Profile of the Zirconia-Yttria Case

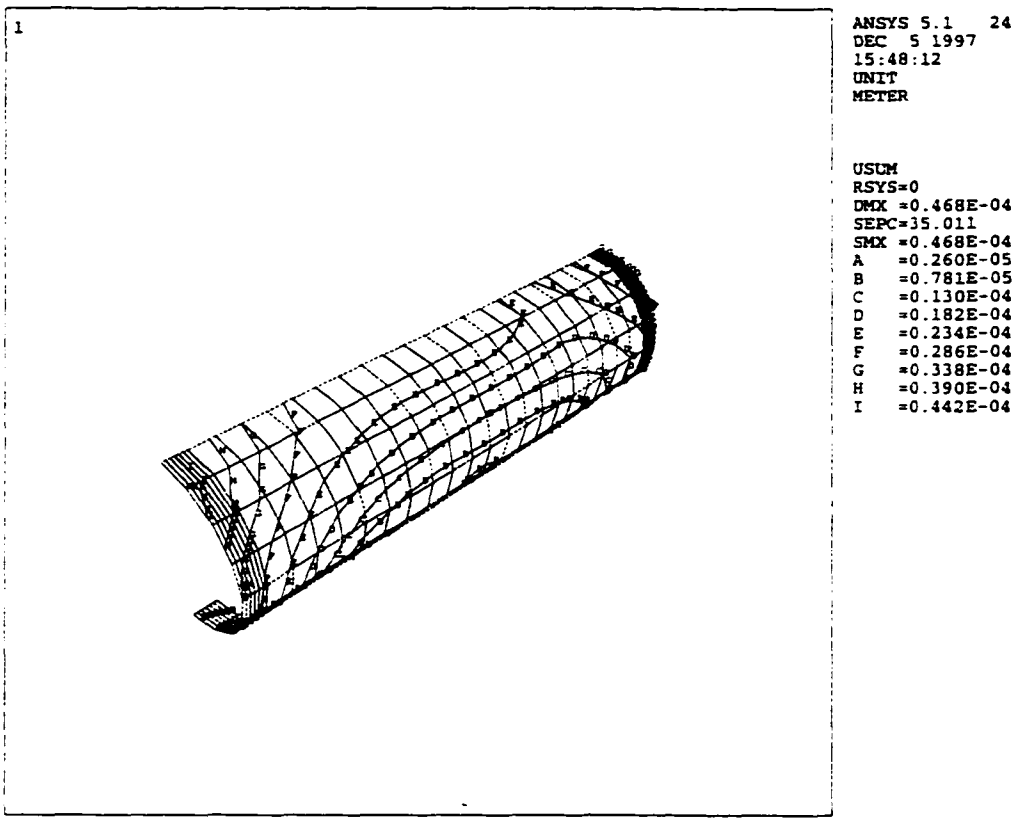

Figure 6.5 Total Displacement Profile of the Alumina Case

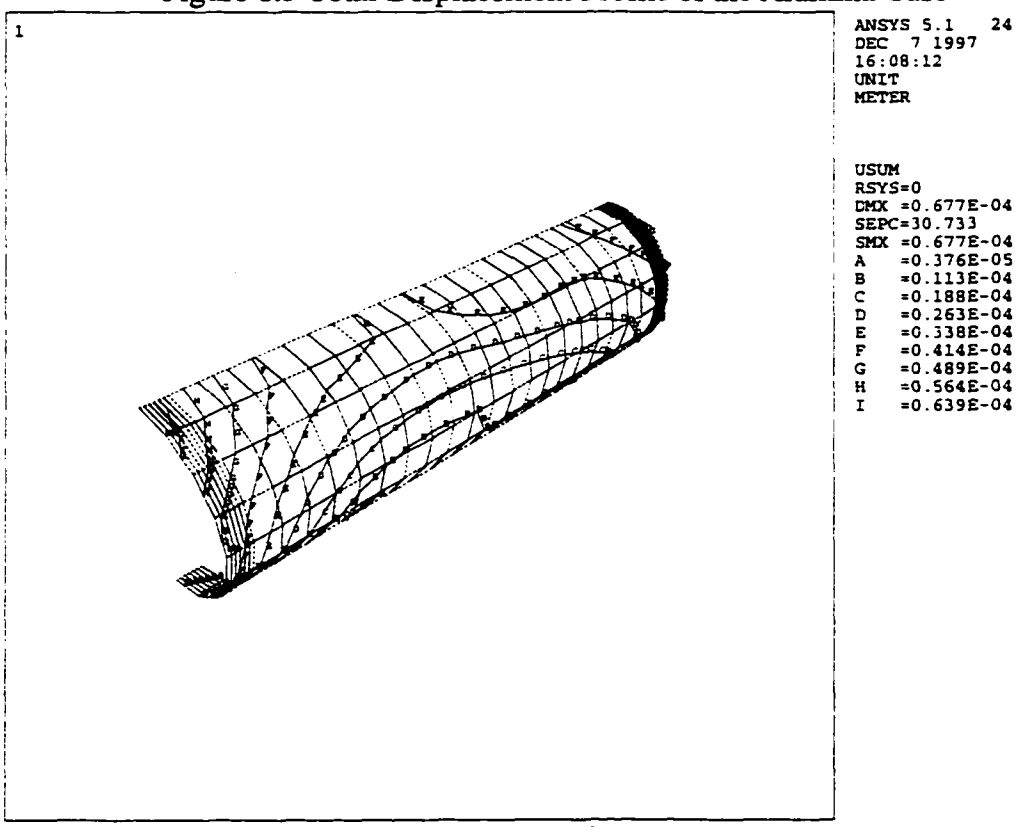

Figure 6.6 Total Displacement Profile of the Zirconia-Yttria Case

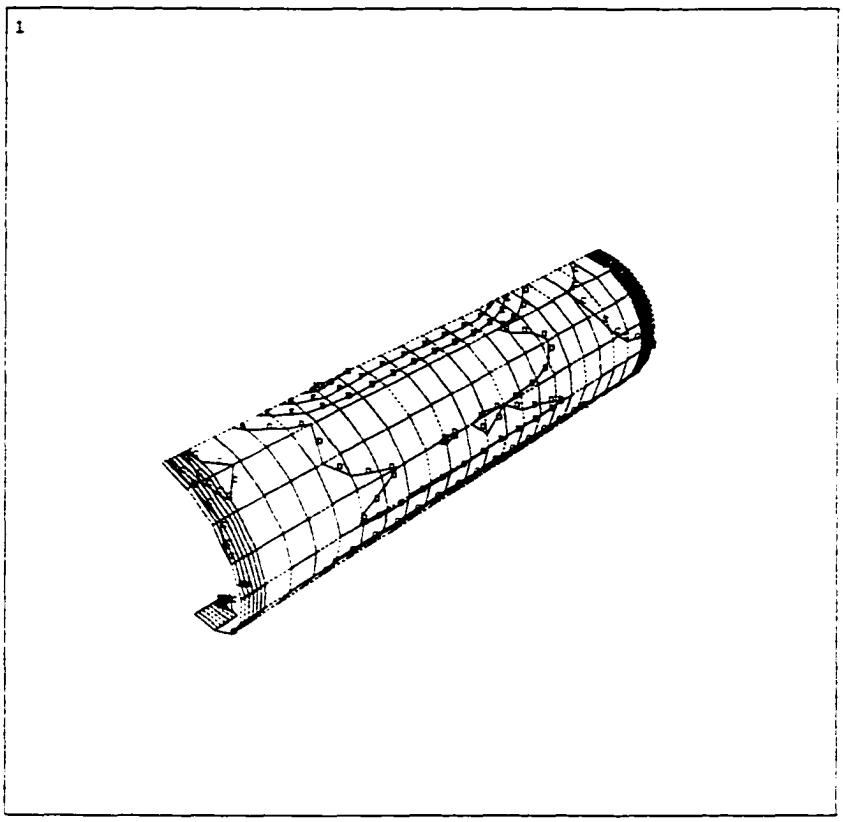

Figure 6.7 First Principal Stress Profile of the Alumina Case

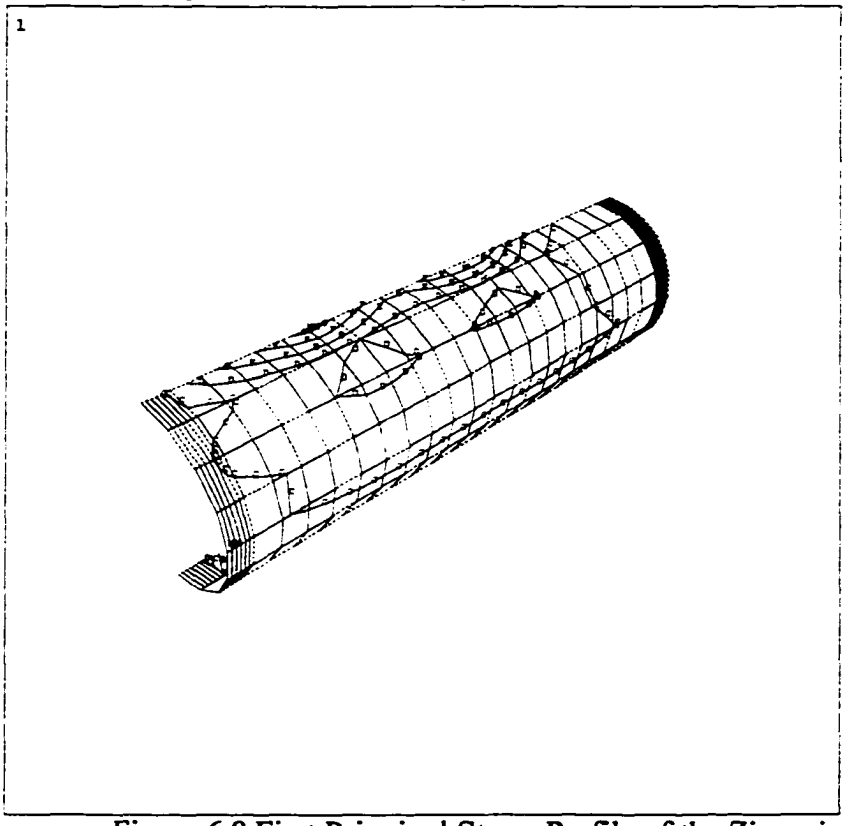

Figure 6.8 First Principal Stress Profile of the Zirconia-Yttria Case

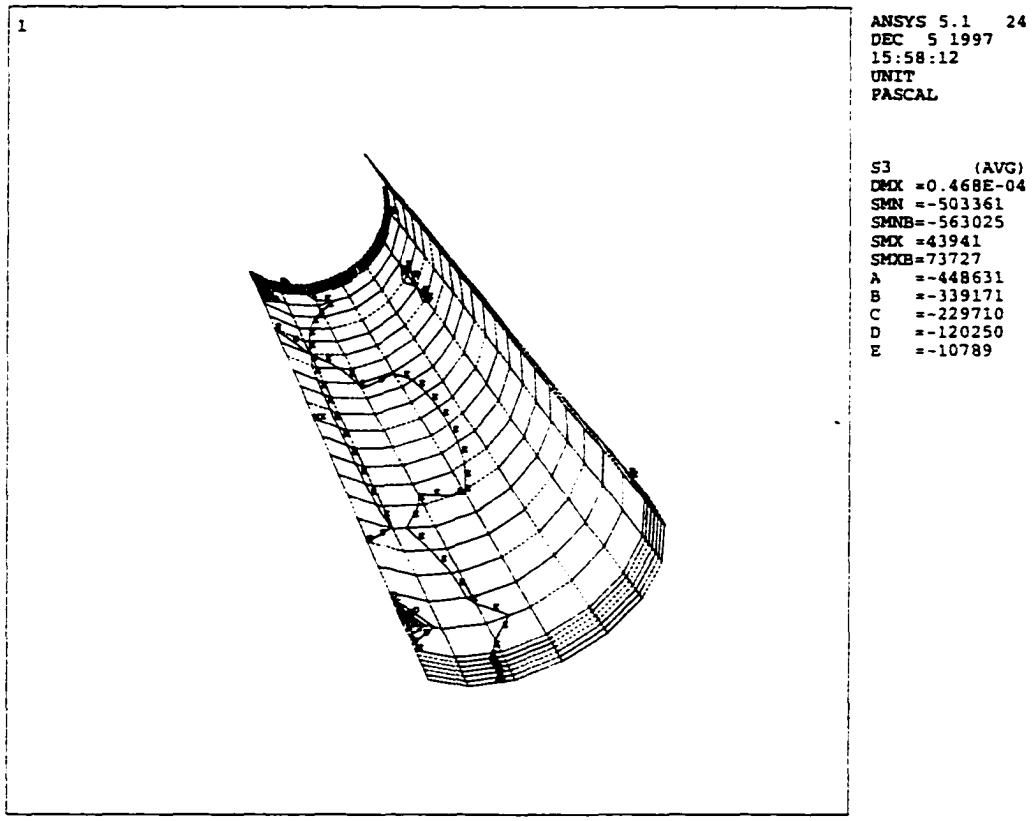

Figure 6.9 Third Principal Stress Profile of the Alumina Case

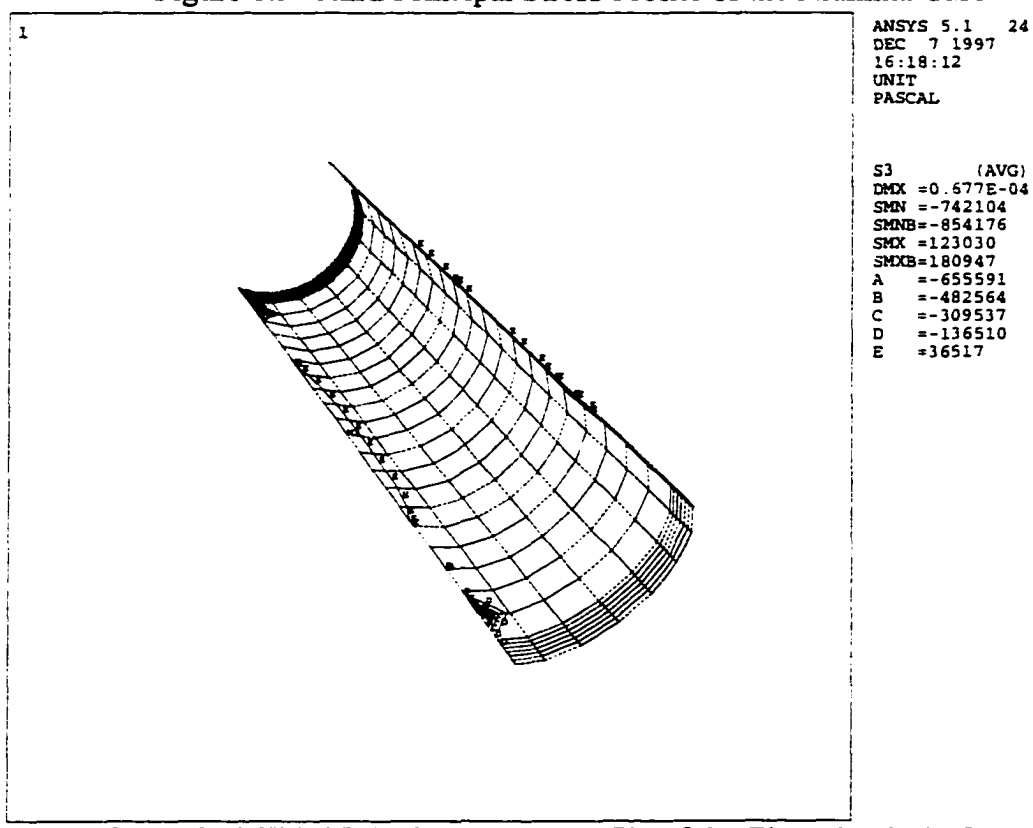

Figure 6.10 Third Principal Stress Profile of the Zirconia-Yttria Case

The maximum temperature from the metal thermal analysis is 26.91 °C for C-22 alloy (Figure 6.11). The maximum total displacement from this thermal stress analysis is 4.91×10^{-5} m (Figure 6.12). The maximum tensile and compressive stresses from this analysis are the first and third principal stresses respectively. The stress value for the first principal stress is 5.91 MPa (Figure 6.13) and the third principal stress value is -2.38 MPa (Figure 6.14). These stresses do not exceed the compressive strength and tensile strength of the C-22 alloy and adhesive strength of the interface. The maximum shear stress value from this analysis is 4.15 MPa. This maximum shear stress value does not exceed half of the adhesive strength value. Hence, the thermal stress from the spent nuclear fuel being placed in C-22 alloy coated waste package has no impact on the bond between the coating and the waste package corrosion allowance barrier.

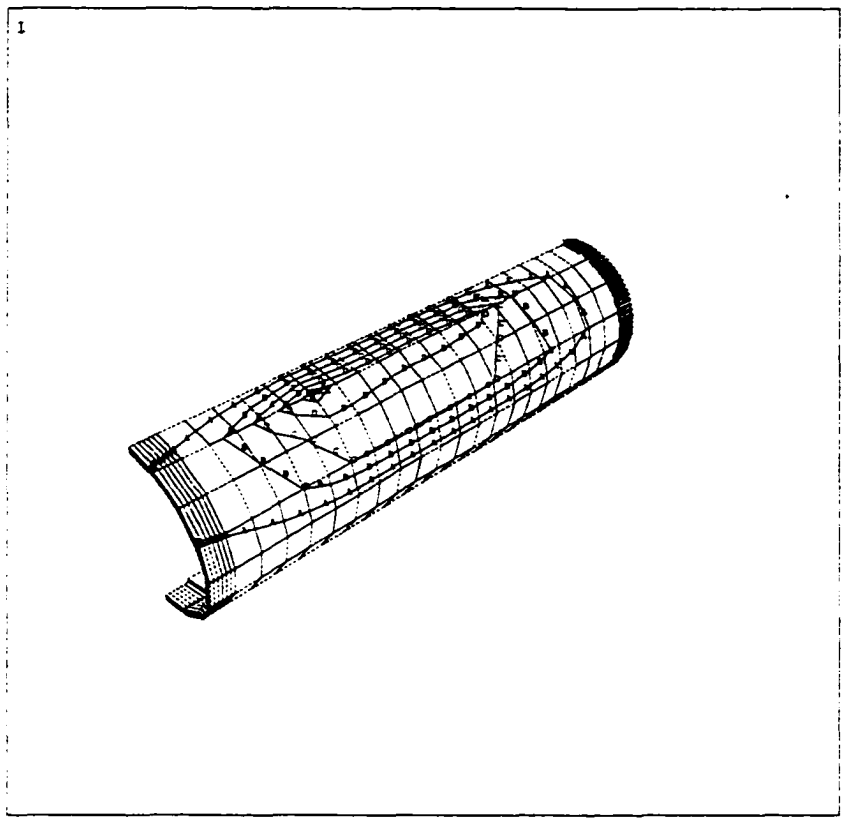

Figure 6.11 Temperature Profile of the C-22 Alloy Case

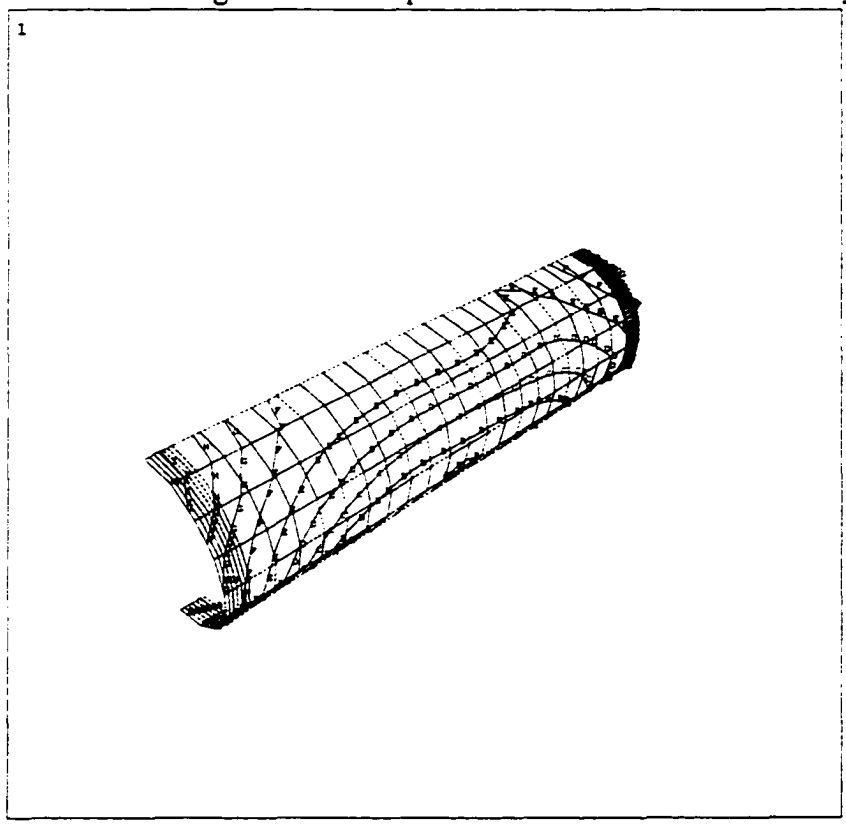

Figure 6.12 Total Displacement Profile of the C-22 Alloy Case

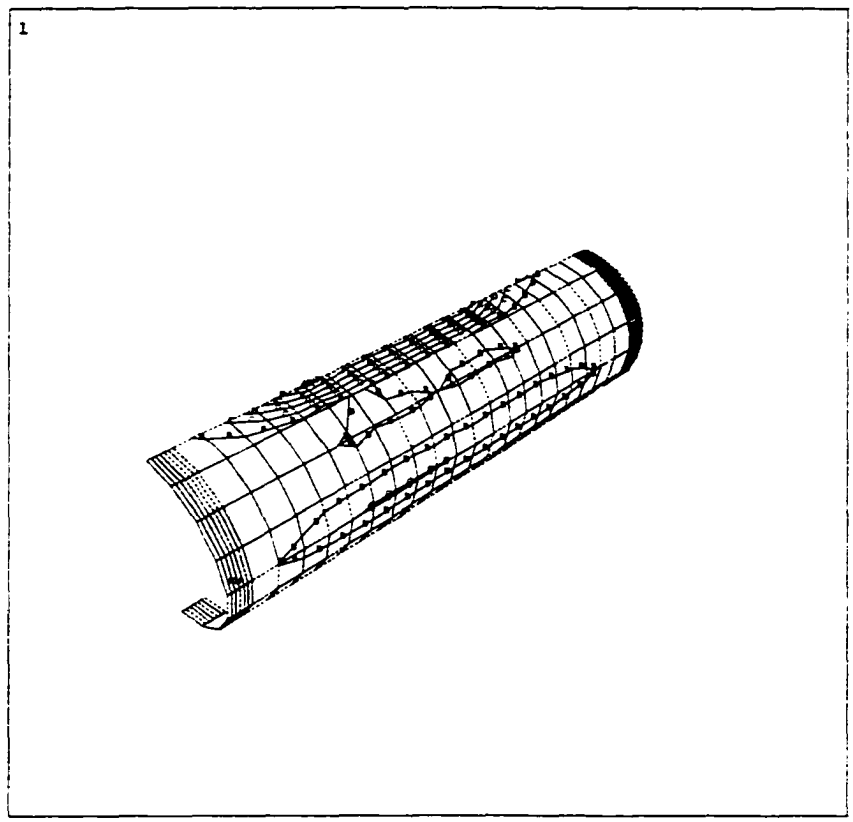

Figure 6.13 First Principal Stress Profile of the C-22 Alloy Case

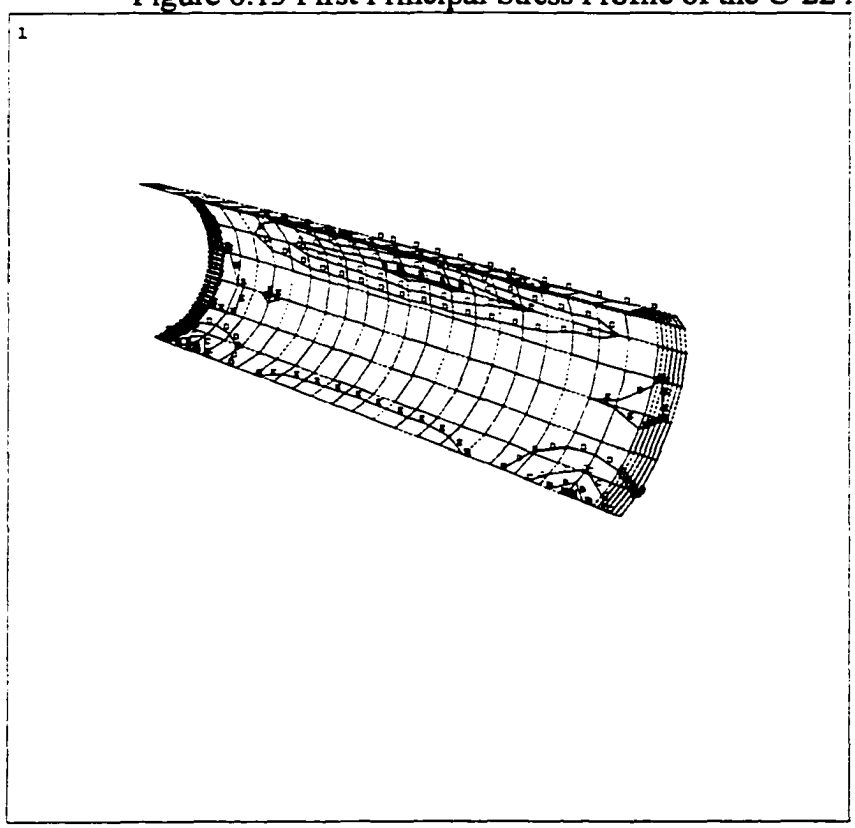

Figure 6.14 Third Principal Stress Profile of the C-22 Alloy Case

The maximum temperatures from the thermal analysis for the FGMs are 26.15°C for alumina FGM (Figure 6.15) and 26.74°C for zirconia-yttria FGM (Figure 6.16). The maximum total displacement from the thermal stress analysis is 2.96×10^{-5} m for alumina FGM (Figure 6.17) and 4.39×10^{-5} m for zirconia-yttria FGM (Figure 6.18). The maximum tensile and compressive stresses from these analyses are the first and third principal respectively. The stress values for the first principal stresses are 2.15 MPa for alumina FGM (Figure 6.19) and 2.21 MPa for zirconia-yttria FGM (Figure 6.20) and the third principal stresses are -0.982 MPa for alumina FGM (Figure 6.21) and -1.01 MPa for zirconia-yttria FGM (Figure 6.22). These stresses do not exceed the compressive strength and tensile strength of the alumina FGM and the zirconia-yttria FGM and the adhesive strength of the interface. The maximum shear stress values are 1.57 MPa for alumina FGM and 1.61 MPa for zirconia-yttria FGM. These stresses do not exceed half the adhesive strength value of the interface. Thus, the thermal stress from the spent nuclear fuel being placed in an alumina FGM or zirconia-yttria FGM coated waste package also has no impact on the bond between the coating and the waste package corrosion allowance barrier.

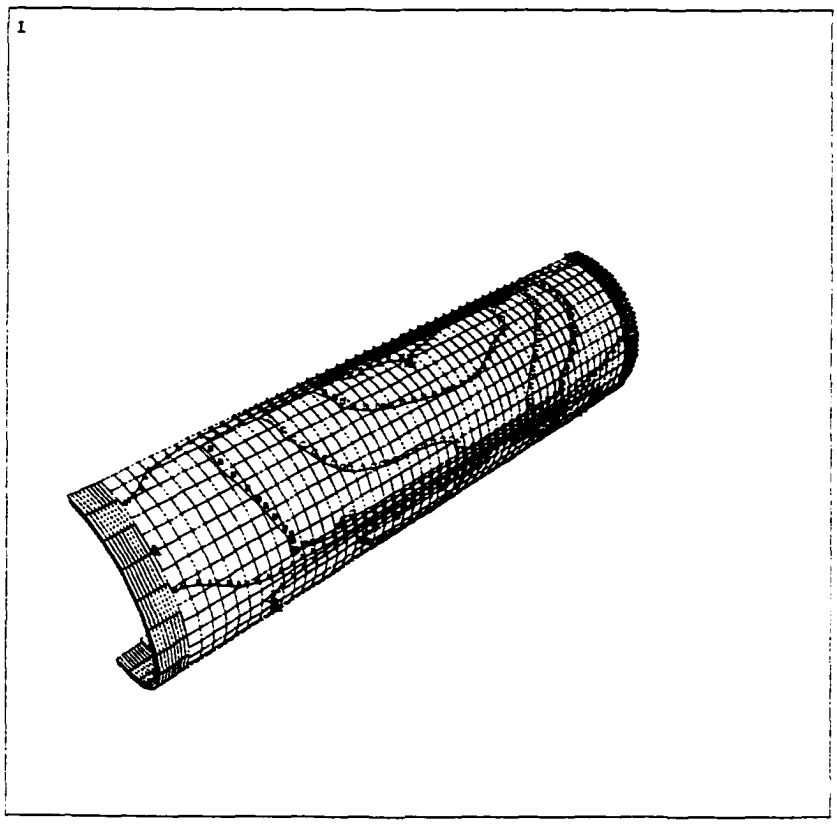

Figure 6.15 Temperature Profile of the Alumina FGM Case

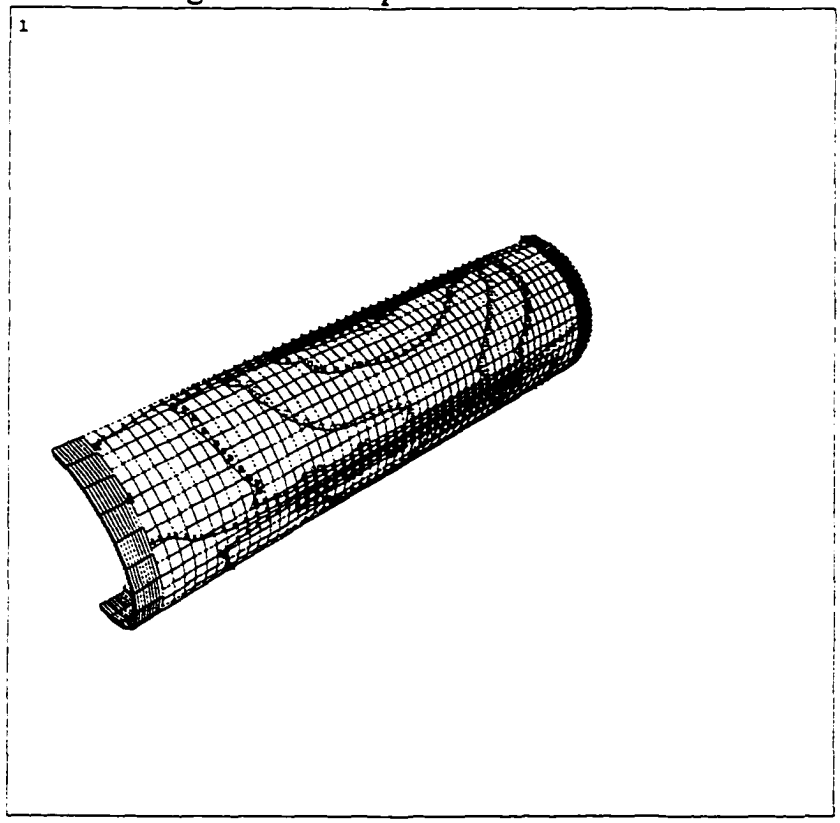

Figure 6.16 Temperature Profile of the Zirconia-Yttria FGM Case

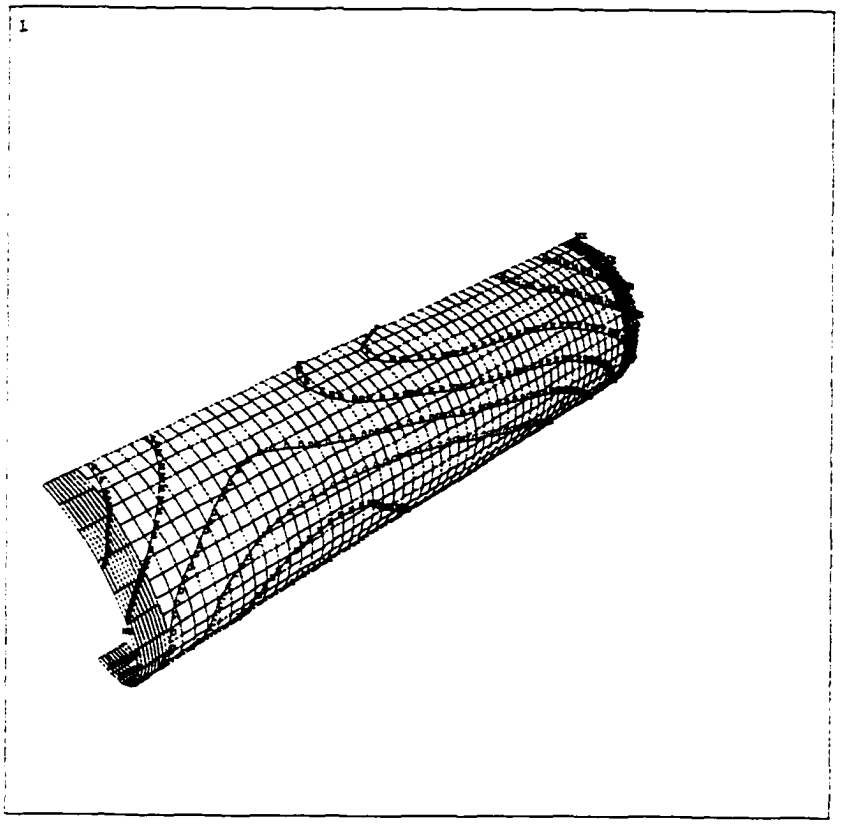

Figure 6.17 Total Displacement Profile of the Alumina FGM Case

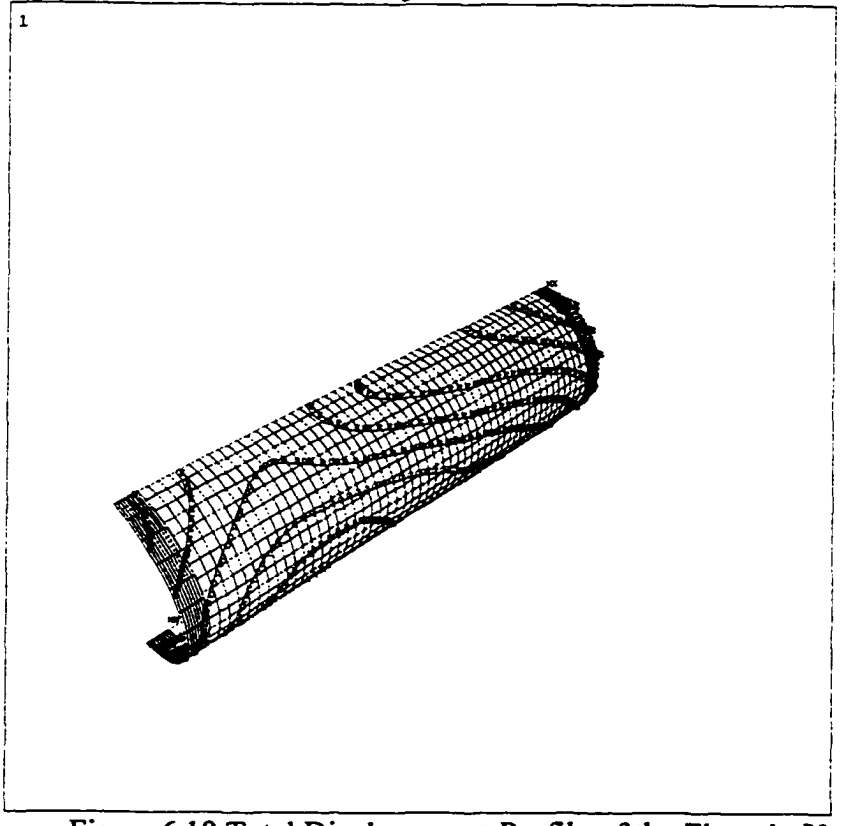

Figure 6.18 Total Displacement Profile of the Zirconia-Yttria FGM Case

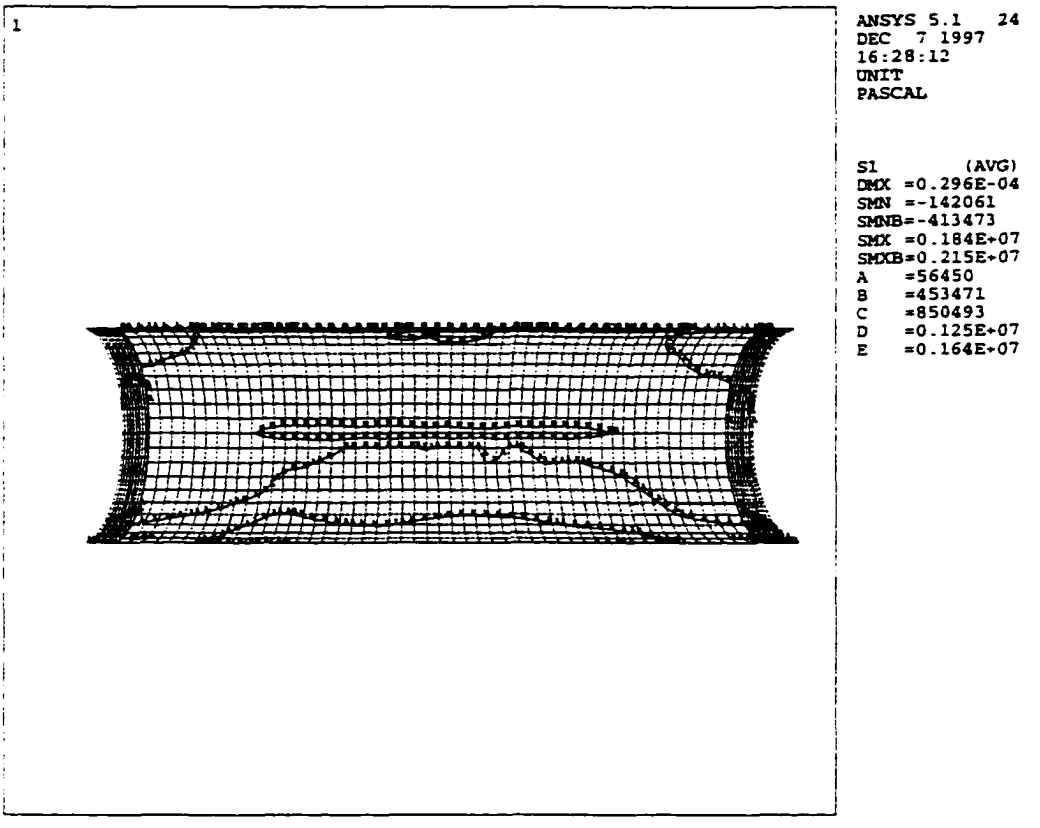

Figure 6.19 First Principal Stress Profile of the Alumina FGM Case

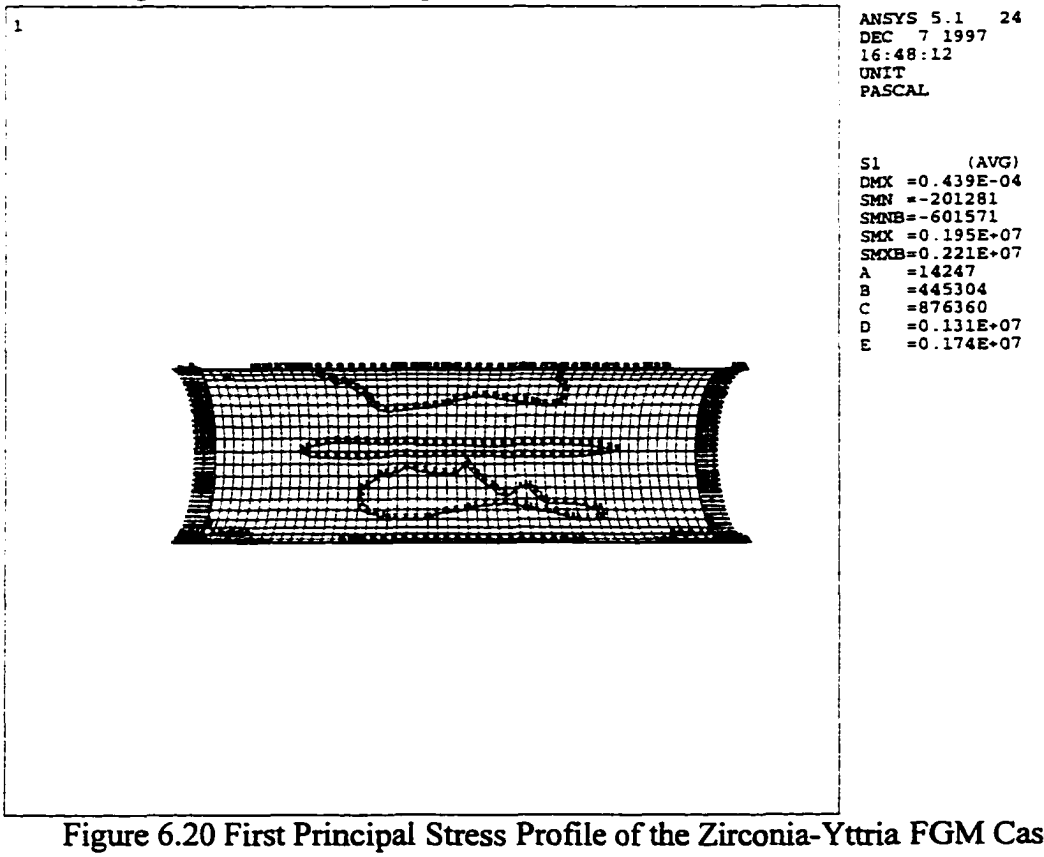

Figure 6.20 First Principal Stress Profile of the Zirconia-Yttria FGM Case

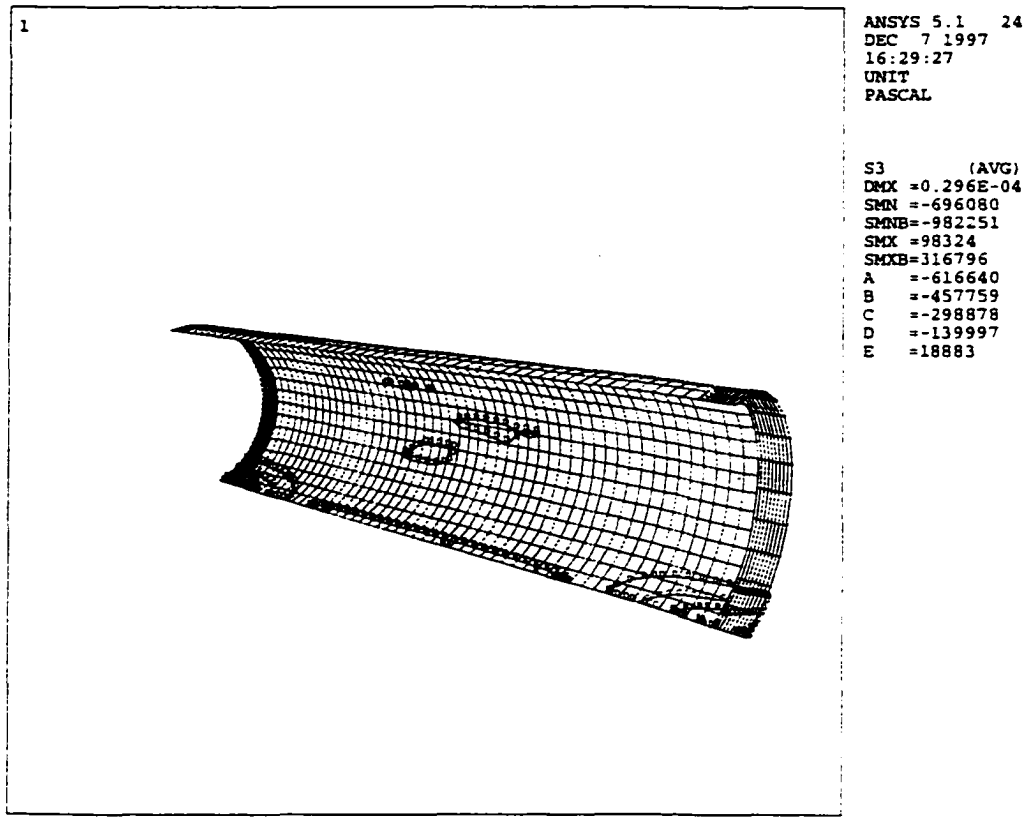

Figure 6.21 Third Principal Stress Profile of the Alumina FGM Case

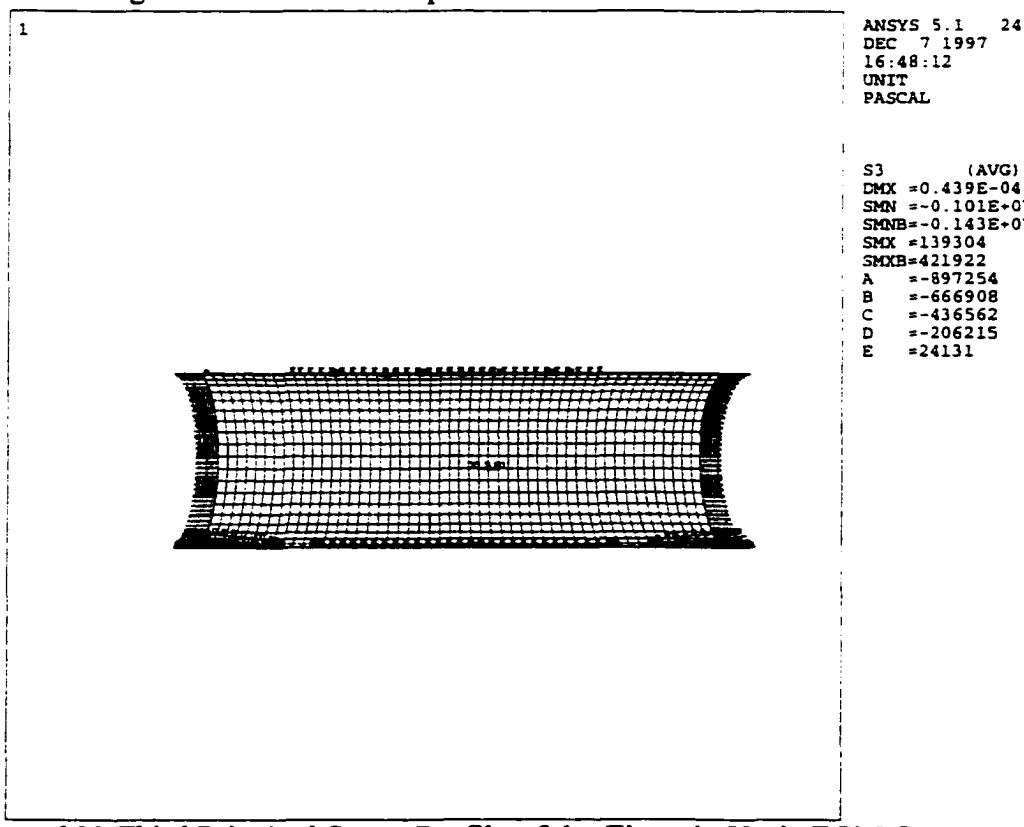

Figure 6.22 Third Principal Stress Profile of the Zirconia-Yttria FGM Case

CHAPTER 7

CONCLUSION

This thesis deals with thermal effects of a large, coated cylinder by a thermal spray process. The large cylinder used in this thesis is a waste package designed to store spent nuclear fuel in an underground repository for tens of thousands of years. The thesis describes the thermal spray process and three thermal spray systems. The next section describes the three material types that can be used as the coating materials to be thermal sprayed on the waste package. The residual stress from the thermal spray process is a thermal effect that is analyzed by two methods and these methods are compared to each other in this thesis. The thermal stress produced by placing spent nuclear fuel into the waste package makes the final section of this thesis.

The thermal spray coating system is made up of several steps. The first step is to heat up the coating material to a semi-molten or molten state. The next step is to spray this coating material at very high velocity to form a mechanical bond onto the substrate. The two methods on how to heat up the coating material are gas combustion and conversion of electrical energy. The gas combustion systems investigated for coating the waste package are the HVOF system and the D-gun system, while the plasma spray system is the candidate system for the conversion of electrical energy method.

Three material classes are developed that might be used as a coating onto the

waste package to prevent the moisture contacting the spent nuclear fuels. These classes are ceramics, metals, and FGMs. The ceramic class is chosen for its low corrosion rates compared to metals. The metal is composed of a corrosion resistant material that has better thermal and mechanical properties than ceramics. The last class is a hybrid combining a metal substrate and ceramic coating to allow better adhesion between the substrate and the coating.

The residual stress section of this analysis compared a mathematical model and a two-dimensional FEA model of applying the coating onto the waste package. The first comparison is the interface temperature during the thermal spray process. The two interface temperatures from these methods are about the same value and within the acceptable percent difference range of $\pm 10\%$. The residual stress that is produced from these two methods shows a very high percent error between the two methods in all three cases. This high percent difference is based on the complexity of the methods. The mathematical model is a simple one-dimensional equation while the FEA model is one-dimensional with more constraints than the mathematical model. Therefore, the mathematical model for residual stress should be used as an approximation to the solution; if a more detailed solution is needed then the one-dimensional FEA model for residual stress should be used.

Finally, the thermal stress of placing spent nuclear fuel into the waste package is analyzed. This analysis used a three-dimensional FEA model of the waste package corrosion allowance barrier with a coating. This model has a variable heat flux applied across the length of the waste package, and the materials from all three material classes were considered as the coating material. The results from this analysis show that in every

case, stresses from this thermal stress will not spall the coating from the substrate. A comparison shows that the ceramic coatings had the lowest tensile, compressive, and shear stresses. The FGMs coatings had the second lowest tensile, compressive, and shear stress values, and the metal coating had the highest tensile, compressive, and shear stress values.

The results of the residual stress analysis and thermal stress analysis indicate that the ceramic coated waste packages have the lowest stress values from the three material groups. At this stage in the design of the thermal sprayed waste package there cannot be a decision made on the type of coating material. This decision can only be made after studies have been performed on the effects of corrosion, handling loads, and accident scenarios that a thermal sprayed waste package may face. Also, a fabrication program needs to be developed to find the best method to coat the waste package if the thermal spray process is feasible.

REFERENCES

1. Krepski R. P. Thermal Spray Coating Applications in the Chemical Process Industries. Houston, TX: NACE International, 1993.
2. Chandler P. E., Quigley M. B. "The Application of Plasma Sprayed Coatings for the Protection of Boiler Tubing." Proceedings of the 11th International Thermal Spray Conference, 1986.
3. Beardsley M. B. "Thick Thermal Barrier Coatings for Diesel Engines." Journal of Thermal Spray Technology 2 (1997): 181-186.
4. Arata Y., Ohmori A., Li C. J. "Study on the Structure of Plasma Sprayed Ceramic Coating Using Copper Electroplating." Proceedings of the International Symposium on Advanced Thermal Spray Technology and Allied Coatings, 1988.
5. Tucker R. C. "ASM International Thermal Spray Workshop." Materials Congress, 2 Oct 1989.
6. Naval Ordnance Station. A Plasma Flame Spray Handbook. Louisville, KY: Naval Ordnance Station, 1977.
7. Rao K. V., Somerville D. A., Lee D. A. "Properties and Characterization of Coatings Made Using Jet Kote Thermal Spray Technique." Proceedings of the 11th International Thermal Spray Conference, 1986.
8. Gansert D. J., Herman H. "Jet-Kote Sprayed Machine Element Coatings."

Proceedings of the National Thermal Spray Conference, 1988.

9. Drzeniek, Steffens H. D. "Cored Tube Wires for Arc and Flame Spraying." Proceedings of the National Thermal Spray Conference, 1987.
10. Bernecki T. F. "Coatings for Aggressive Environments." ASM Materials Congress, 1989.
11. Unger R. "Comparison of Thermal Spray Bond Coats." Proceedings of the National Thermal Spray Conference, 1987.
12. Juvinall R. C., Marshek K. M. Fundamentals of Machine Component Design, Second Edition. New York, NY: John Wiley & Sons, 1991.
13. Stover D., Jager D. A., Schutz H. G. "Residual Stresses in Low Pressure Plasma Sprayed Chromia Coating." Proceedings of the National Thermal Spray Conference, 1991.
14. Electric Power Research Institute. Testing and Analyses of the TN-24P PWR Spent-Fuel Dry Storage Cask Loaded with Consolidated Fuel. EPRI NP-6191. Richland, WA: EPRI, 1989.
15. Wang H. Thermal Evaluation of the 21 PWR UCF Waste Package with an Additional Barrier. CRWMS M&O Report No. BBAA00000-01717-0200-0024 REV 00. Las Vegas, NV: CRWMS M&O, 1997.
16. Ceylan Z. Rock Fall Analysis of an Additional Barrier on UCF WP. CRWMS M&O Report No. BBAA00000-01717-0200-00023 REV 00. Las Vegas, NV: CRWMS M&O, 1997.
17. Swanson Analysis Systems, Inc. ANSYS User's Manual for Revision 5.1 Volume IV Theory. Houston, PA: SAS IP, 1994.

18. Williamson R. L., Rabin B. H., Drake J. T. Finite Element Analysis of Thermal Residual Stresses at Graded Ceramic-Metal Interfaces. Part I. Model Description and Geometrical Effects. Idaho National Engineering Laboratory Report. Idaho Falls, ID: EG&G Idaho, Inc., 1993.

APPENDIX A

MATERIALS PROPERTIES

Table A.1 Material Properties for the Corrosion Allowance Barrier, Ceramic, and Metallic Coatings

Properties	ASTM A 516 Grade 70 (15,16)	Alumina (15,16)	Zirconia-Yttria (15,16)	C-22 Alloy (15,16)
Density (kg/m^3)	7850	3230	5400	8691.6
Poisson's ratio	0.3	0.21	0.23	0.286
Young's modulus (GPa)	190	13	20	203
Yield strength (MPa)	225	N/A	N/A	N/A
Coefficient of thermal expansion ($x10^{-6}$ m/m°C)	13.1	9	8.04	12.4
Thermal conductivity (W/m°C)	40.84	22.4	1.5	10.1
Emissivity	0.80	0.3	0.4	0.87
Tensile strength (MPa)	N/A	27.2	27.2*	765
Adhesive strength (MPa)	N/A	14.2	14.2*	14.2*
Compressive Strength (MPa)	N/A	2100	2089	1530

*Material properties with an asterisk are assumed to use the material properties of alumina.

The FGMs' mechanical and thermal properties are derived from calculations in Appendix C. The adhesive, compressive, tensile strength values for these FGMs are the strength values of the ceramic that makes up that peculiar FGM.

Table A.2 Material Properties for the Alumina FGM Coating

Properties	Layer 1 (75% substrate - 25 % ceramic)	Layer 2 (50% substrate - 50% ceramic)	Layer 3 (25% substrate - 75% ceramic)
Density (kg/m^3)	6695	5540	4385
Poisson's ratio	0.277	0.255	0.232
Young's Modulus (GPa)	145.8	101.5	57.25
Coefficient of thermal expansion ($x10^{-6}$ m/m°C)	12.07	11.05	10.03
Thermal conductivity (W/m°C)	36.23	31.62	27.01
Emissivity	0.675	0.55	0.425

Table A.3 Material Properties for the Zirconia-Yttria FGM Coating

Properties	Layer 1 (75% substrate - 25 % ceramic)	Layer 2 (50% substrate - 50% ceramic)	Layer 3 (25% substrate - 75% ceramic)
Density (kg/m^3)	7248	6645	4385
Poisson's ratio	0.282	0.265	0.232
Young's Modulus (GPa)	147.5	105	62.5
Coefficient of thermal expansion ($x10^{-6}$ m/m°C)	11.83	10.57	9.31
Thermal conductivity (W/m°C)	31.01	21.17	11.34
Emissivity	0.7	0.6	0.5

APPENDIX B

FINITE ELEMENT ANALYSIS PROCEDURE

The FEA of this thesis used a commercial software program called ANSYS. Appendix B describes the analysis procedure of the ANSYS software. The description of this procedure and the equations are from ANSYS User's Manuel for Revision 5.1, Volume IV Theory(17).

The ANSYS FEA uses a matrix displacement method. The item being analyzed must be made up of discrete regions that are called elements. These discrete regions are connected at a finite number of points that are called nodes. If the "force-displacement" relationship for each element ("stiffness" matrix) is known then the "force-displacement relationships" for the entire "structure" can be assembled using standard matrix methods. Thermal analyses are done in an analogous basis.

STATIC ANALYSIS

Assumptions and Restrictions:

It is valid for all degrees of freedom (DOFs). Inertial and damping effects are ignored, except for static acceleration fields.

Description of Structural Systems:

The overall equilibrium equations for linear structural static analysis are:

$$[K]\{u\} = \{F\} \tag{B.1}$$

or

$$[K]\{u\} = \{F^a\} + \{F^r\} \tag{B.2}$$

where $[K]$ = total stiffness matrix = $\sum_{m=1}^{N}[K_e]$, $\{u\}$ = nodal displacement vector, N = number of elements, $[K_e]$ = element stress matrix (may include the element stress stiffness matrix), $\{F^r\} = [K]\{u\} - \{F^{nd}\} - \{F^e\}$ = reaction load vector, $\{F^{nd}\}$ = applied nodal load vector, and $\{F^e\}$ = total of all element load vector effects (pressure, acceleration, thermal, gravity). $\{F^a\}$, the total applied load vector, is defined by:

$$\{F^a\} = \{F^{nd}\} + \{F^{ac}\} + \sum_{m=1}^{N}(\{F_e^{th}\} + \{F_e^{pr}\}) \tag{B.3}$$

where $\{F^{nd}\}$ = applied nodal load vector, $\{F^{ac}\} = -[M]\{a_c\}$ = acceleration load vector, $[M]$ = total mass matrix = $\sum_{m=1}^{N}[M_e]$, $[M_e]$ = element mass matrix, $\{a_c\}$ = total acceleration vector, $\{F_e^{th}\}$ = element thermal load vector, and $\{F_e^{pr}\}$ = element pressure load vector.

Description of Thermal Systems:

The overall equations for a linear thermal system are the same as for a linear structural static analysis, Equation B.1 and Equation B.2. [K], though, is the total coefficient matrix like the total conductivity matrix = $[K^{tm}_e]+[K^{tb}_e]+[K^{tc}_e]$, $[K^{tm}_e] = \rho\int_{vol} c\{N\}\{v\}^T[B]d(vol)$ = element mass transport conductivity matrix, $[K^{tb}_e] = \int_{vol}[B]^T[D][B]d(vol)$ = element diffusion conductivity matrix,

$[K^{tc}_e] = \int_{S3} h_f\{N\}\{N\}^T d(S3)$ = element convection surface conductivity matrix, h_f = film coefficient, S3 = specified convection surfaces acting over surface S3 (Newton's law of cooling), and {u} is the nodal temperature value = {T}. $\{Q^f\}$, the total heat flux vector, is defined by:

$$\{Q^f\} = \{Q^{nd}\} + \sum_{m=1}^{N} (\{Q_e\} + \{Q_e^g\} + \{Q_e^c\}) \qquad \text{(B.4)}$$

where $\{Q^{nd}\}$ = applied nodal heat flow vector, $\{Q_e\} = \int_{S2} \{N\}q^* d(S2)$ = element heat flux vector, q^* = specified heat flow, S2 = specified heat flows acting over surface S2, $\{Q_e^g\} = \int_{vol} q'''\{N\}d(vol)$ = element heat generation rate vector, $\{Q_e^c\} = \int_{S3} T_b h_f\{N\}d(S3)$ = element convection surface vector, and T_B = bulk temperature of the adjacent fluid.

APPENDIX C

CALCULATIONS

The Interface Temperature of metal substrate and ceramic coating at ambient temperature for Chapter 5:

TI = Interface Temperature

dM = Metal Thickness = .1 m

q = heat flux = 1*10^6 W/m^2

TM = Temperature Metal = 25 C = 298.15 K

kM = 40.84 W/mK

$TM = 298.15 \quad q = 1 \cdot 10^{6} \quad dM = .1 \quad kM = 40.84$

$$TI = \frac{q}{kM} \cdot dM + TM$$

$TI = 2.747 \cdot 10^{3}$

$TIC = TI - 273.15 \qquad TIC = 2.474 \cdot 10^{3}$ TIC = Interface Temperature in C

Thermal Stresses at Thermal Spraying for Alumina, Zirconia-Yttria, and C-22 Alloy at the Interface:

E= Young's Modulus: Ealumina = 13 GPa; Ezirconia = 20 GPa; EC-22 = 203 GPa

v = Poisson's Ratio: valumina = 0.21; vzirconia = 0.23; vC-22 = 0.286

alpha = Thermal Expansion coefficient: alphametal = 13.1*10^-6 /C; alphaalumina = 9*10^-6/C; alphazirconia = 8.04*10^-6/C; alphaC-22 = 12.4*10^-6/C

T = Temperature at which stress is measured (normally ambient temperature)

sigma I = Stress at Interface in Pascal

$i = 0..2$

$E_i = \qquad v_i = \qquad \alpha M = 13.1 \cdot 10^{-6} \qquad \alpha C_i = \qquad T = 25$

E_i
$13 \cdot 10^{9}$
$20 \cdot 10^{9}$
$203 \cdot 10^{9}$

v_i
0.21
0.23
0.286

αC_i
$9 \cdot 10^{-6}$
$8.04 \cdot 10^{-6}$
$12.4 \cdot 10^{-6}$

$$\sigma I_i = \frac{E_i}{(1 - v_i)} \cdot (\alpha M - \alpha C_i) \cdot (T - TIC)$$

σI_i

σI_i
$-1.652 \cdot 10^{8}$
$-3.218 \cdot 10^{8}$
$-4.873 \cdot 10^{8}$

Average Residual Stress at the Interface from the Model for Table 5.1:

Residual Stress is in units of Pascals:

$i = 0..14$

$\sigma Al2O3_i$ =	$\sigma C22_i$ =	$\sigma ZrO2_i$ =
$-7.77 \cdot 10^7$	$-2.80 \cdot 10^9$	$-6.70 \cdot 10^7$
$-3.41 \cdot 10^7$	$-1.40 \cdot 10^9$	$-2.77 \cdot 10^7$
$-5.56 \cdot 10^7$	$-1.94 \cdot 10^9$	$-4.82 \cdot 10^8$
$-8.93 \cdot 10^4$	$-4.02 \cdot 10^8$	$4.39 \cdot 10^6$
$-3.41 \cdot 10^7$	$-8.80 \cdot 10^8$	$-2.72 \cdot 10^7$
$-7.55 \cdot 10^7$	$-2.69 \cdot 10^9$	$-6.57 \cdot 10^7$
$2.23 \cdot 10^7$	$2.61 \cdot 10^7$	$2.81 \cdot 10^7$
$-1.96 \cdot 10^7$	$-1.43 \cdot 10^8$	$-2.04 \cdot 10^7$
$2.27 \cdot 10^7$	$-3.57 \cdot 10^8$	$3.58 \cdot 10^7$
$-3.33 \cdot 10^7$	$-1.67 \cdot 10^8$	$-3.66 \cdot 10^7$
$8.16 \cdot 10^6$	$-1.33 \cdot 10^9$	$2.14 \cdot 10^7$
$-6.31 \cdot 10^7$	$-9.36 \cdot 10^8$	$-6.55 \cdot 10^7$
$-1.93 \cdot 10^7$	$-2.34 \cdot 10^9$	$-3.67 \cdot 10^6$
$-8.56 \cdot 10^7$	$-1.98 \cdot 10^9$	$-8.23 \cdot 10^7$
$-1.27 \cdot 10^8$	$-2.77 \cdot 10^9$	$-1.27 \cdot 10^8$

$\sigma avgAl = mean(\sigma Al2O3)$ $\sigma avgC22 = mean(\sigma C22)$ $\sigma avgZr = mean(\sigma ZrO2)$

$\sigma avgAl = -3.81 \cdot 10^7$ $\sigma avgC22 = -1.34 \cdot 10^9$ $\sigma avgZr = -6.1 \cdot 10^7$

Percent differences between the mathematical model and the FEA in Chapter 5:

Percent difference is based on the absolute value of the difference of the two models divided by the mathematical model:

Interface Temperature Percent Difference

TImath = 2474 TIFEA = 2636

$$\%TI = \frac{|TImath - TIFEA|}{TImath} \cdot 100$$

%TI = 6.548

Alumina Percent Difference:

Almath = -165 AlFEA = -38.1

$$\%Al = \frac{|Almath - AlFEA|}{|Almath|} \cdot 100$$

%Al = 76.909

Zirconia-Yttria Percent Difference:

Zrmath = -322 ZrFEA = -61

$$\%Zr = \frac{|Zrmath - ZrFEA|}{|Zrmath|} \cdot 100$$

%Zr = 81.056

C-22 Alloy Percent Difference:

C22math = -487 C22FEA = -1340

$$\%C22 = \frac{|C22math - C22FEA|}{|C22math|} \cdot 100$$

%C22 = 175.154

Variable Heat Flux for Table 6.1:

Q = heat flux (W/m^2)

q = heat transfer rate (W/assy)

N = number of assy in a waste package

L = length of assy (m)

D = inside diameter of the corrosion resistant barrier (m)

rv = relative value

Qv = variable heat flux (W/m^2)

$i := 0..7$

$q := 850.01 \quad N := 21 \quad L := 4 \quad D := 1.4234$

$$Q := \frac{q \cdot N}{\pi \cdot D \cdot L}$$

$Q = 997.945$

$rv_i =$

0.3
1.10
1.21
1.21
1.12
1.25
1.15
0.6

$Qv_i := Q \cdot rv_i$

Qv_i

299.38343
$1.09774 \cdot 10^3$
$1.20751 \cdot 10^3$
$1.20751 \cdot 10^3$
$1.1177 \cdot 10^3$
$1.24743 \cdot 10^3$
$1.14764 \cdot 10^3$
598.76686

One-dimensional heat transfer model taking account of radiation for thermal analysis section in Chapter 6:

First find the radiation heat transfer coefficient:

$i := 0..2$

$q := 1247.43 \quad \varepsilon := 0.3 \quad \sigma := 5.67 \cdot 10^{-8} \quad Tinf_i :=$

293.15
298.15
303.15

$$T3_i := \left[\frac{q}{\varepsilon \cdot \sigma} + \left(Tinf_i\right)^4 \right]^{.25}$$

$T3_i$

533.023
533.874
534.765

$$hr_i := \varepsilon \cdot \sigma \cdot \left(T3_i + Tinf_i\right) \cdot \left[\left(T3_i\right)^2 + \left(Tinf_i\right)^2 \right]$$

hr_i

5.2
5.292
5.386

Find the corrosion allowance barrier inner temperature and the interface temperature by thermal resistance:

$L1 := .1 \quad K1 := 40.84 \quad L2 := .005 \quad K2 := 22.4$

$$R1 := \frac{L1}{K1} \qquad R2 := \frac{L2}{K2} \qquad R3_i := \frac{1}{hr_i}$$

$R1 = 2.449 \cdot 10^{-3}$

$R2 = 2.232 \cdot 10^{-4}$

$R3_i$

0.192
0.189
0.186

$RT_i := R1 + R2 + R3_i$

RT_i

0.195
0.192
0.188

$T1_i = q \cdot RT_i + Tinf_i$

$T1_i$

536.355
537.207
538.098

$T2_i = T1_i - q \cdot R1$

$T2_i$

533.301
534.152
535.043

Find one-dimensional stress values using the residual stress mathematical equation:

$\alpha 1 = 13.1 \cdot 10^{-6} \quad \alpha 2 = 9 \cdot 10^{-6} \quad E2 = 13 \cdot 10^{9} \quad v2 = 0.21$

$$\sigma th_i = \frac{E2}{1 - v2} \cdot (\alpha 1 - \alpha 2) \cdot \left(T2_i - T3_i\right)$$

σth_i

$1.879 \cdot 10^{4}$
$1.879 \cdot 10^{4}$
$1.879 \cdot 10^{4}$

Therefore, radiation heat transfer has no effect on the thermal stress of the waste package.

Determining the mechanical and thermal properties of a FGM is based on volume fraction equations as shown below(16):

FGM Alumina material properties for Table A.2:

$i := 0..2$

$Est := 190 \cdot 10^{9}$ $Eal := 13 \cdot 10^{9}$ $qst := 7850$ $qal := 3230$ $\alpha st := 13.1 \cdot 10^{-6}$ $\alpha al := 9 \cdot 10^{-6}$

$kst := 40.84$ $kal := 22.4$ $\varepsilon st := .8$ $\varepsilon al := .3$ $vst := 0.3$ $val := .21$

$Vst_i :=$ $Vc_i :=$

Vst_i	Vc_i
.75	.25
.50	.50
.25	.75

$Efgm_i := Vst_i \cdot Est + Vc_i \cdot Eal$ $qfgm_i := Vst_i \cdot qst + Vc_i \cdot qal$ $\alpha fgm_i := Vst_i \cdot \alpha st + Vc_i \cdot \alpha al$

$Efgm_i$	$qfgm_i$	αfgm_i
$1.458 \cdot 10^{11}$	$6.695 \cdot 10^{3}$	$1.207 \cdot 10^{-5}$
$1.015 \cdot 10^{11}$	$5.54 \cdot 10^{3}$	$1.105 \cdot 10^{-5}$
$5.725 \cdot 10^{10}$	$4.385 \cdot 10^{3}$	$1.003 \cdot 10^{-5}$

$kfgm_i := Vst_i \cdot kst + Vc_i \cdot kal$ $\varepsilon fgm_i := Vst_i \cdot \varepsilon st + Vc_i \cdot \varepsilon al$ $vfgm_i := Vst_i \cdot vst + Vc_i \cdot val$

$kfgm_i$	εfgm_i	$vfgm_i$
36.23	0.675	0.277
31.62	0.55	0.255
27.01	0.425	0.232

FGM Zirconia-Yttria material properties for Table A.3:

$i = 0..2$

$Est = 190 \cdot 10^{9}$ $Ezr = 20 \cdot 10^{9}$ $qst = 7850$ $qzr = 5440$ $\alpha st = 13.1 \cdot 10^{-6}$ $\alpha zr = 8.04 \cdot 10^{-6}$

$kst = 40.84$ $kzr = 1.5$ $\varepsilon st = .8$ $\varepsilon zr = .4$ $vst = 0.3$ $vzr = 0.23$

$Vst_i =$ $Vc_i =$

Vst_i	Vc_i
.75	.25
.50	.50
.25	.75

$Efgm_i = Vst_i \cdot Est + Vc_i \cdot Ezr$ $qfgm_i = Vst_i \cdot qst + Vc_i \cdot qzr$ $\alpha fgm_i = Vst_i \cdot \alpha st + Vc_i \cdot \alpha zr$

$Efgm_i$
$1.475 \cdot 10^{11}$
$1.05 \cdot 10^{11}$
$6.25 \cdot 10^{10}$

$qfgm_i$
$7.248 \cdot 10^{3}$
$6.645 \cdot 10^{3}$
$6.043 \cdot 10^{3}$

αfgm_i
$1.183 \cdot 10^{-5}$
$1.057 \cdot 10^{-5}$
$9.305 \cdot 10^{-6}$

$kfgm_i = Vst_i \cdot kst + Vc_i \cdot kzr$ $\varepsilon fgm_i = Vst_i \cdot \varepsilon st + Vc_i \cdot \varepsilon zr$ $vfgm_i = Vst_i \cdot vst + Vc_i \cdot vzr$

$kfgm_i$
31.005
21.17
11.335

εfgm_i
0.7
0.6
0.5

$vfgm_i$
0.282
0.265
0.248

VITA

Graduate College
University of Nevada, Las Vegas

Michael Joseph Plinski

Home Address:
2901 North Rainbow Boulevard Apartment #1068
Las Vegas, NV 89108

Degrees:
Bachelor of Science, Mechanical Engineering, 1995
University of Nevada, Las Vegas

Special Honors and Awards:
Nevada Society of Professional Engineers Foundation Scholarship, 1994-1995
NASA Space Grant Scholarship, 1995
Member of Tau Beta Pi Engineering Honor Society

Thesis Title: Thermal Stress Analysis of Thermally Sprayed Coatings on a Spent Nuclear Fuel Waste Package

Thesis Examination Committee:
Chairperson, Dr. Darrell W. Pepper, Ph.D.
Committee Member, Dr. Brendan J. O'Toole, Ph.D.
Committee Member, Dr. Robert L. Skaggs, Ph.D
Graduate Faculty Representative, Dr. Michelle L. Schultz, Ph.D

IMAGE EVALUATION TEST TARGET (QA-3)

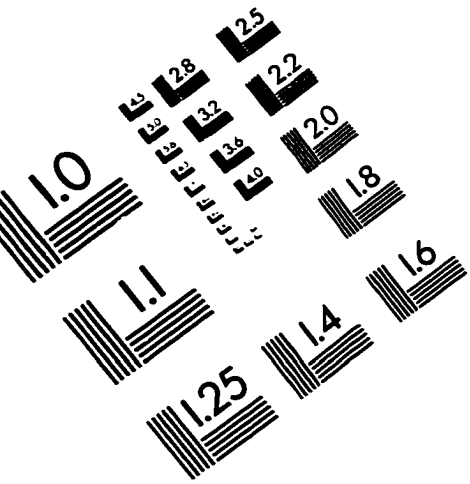

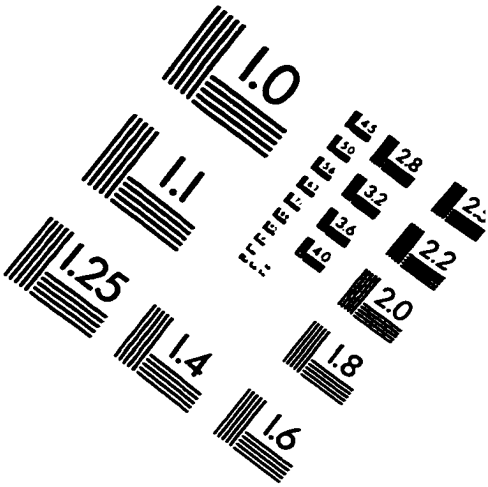

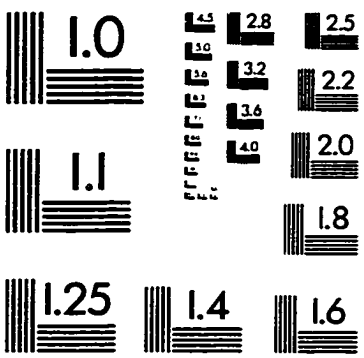

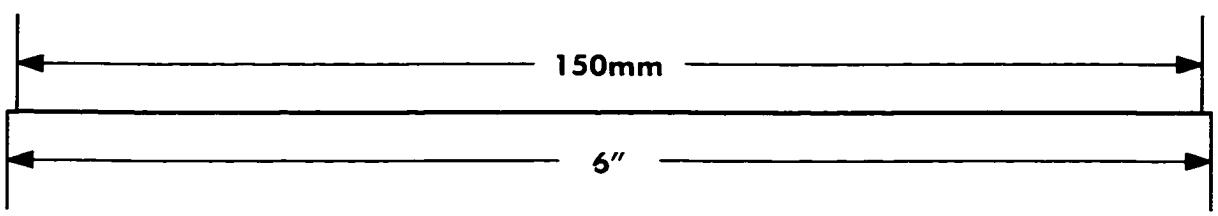

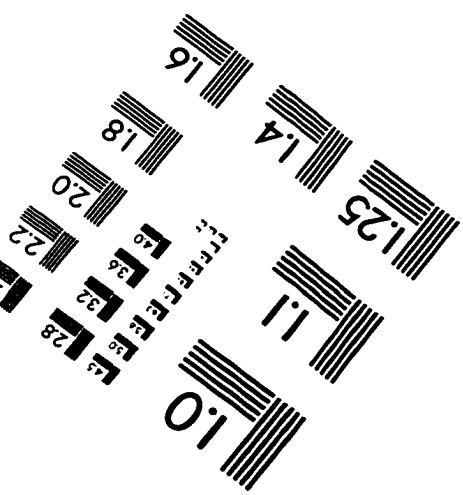

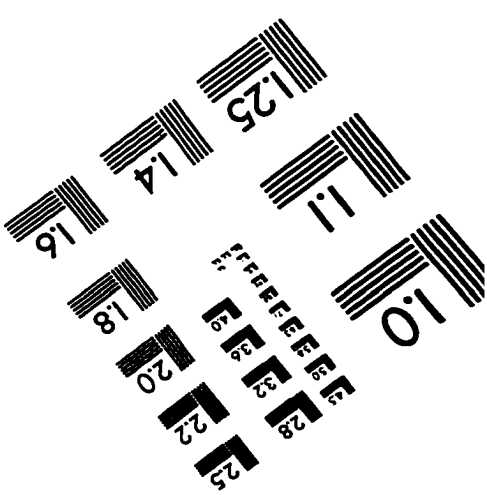

APPLIED IMAGE, Inc
1653 East Main Street
Rochester, NY 14609 USA
Phone: 716/482-0300
Fax: 716/288-5989